Radboud Universiteit Nijmegen

Dynamic Tidal Resonances in Extreme Mass Ratio Inspirals

Investigating the influence of the motion of the perturber

W.E.J. ten Haaf

Supervised by: Dr. Béatrice Bonga

Second reader: Dr. Badri Krishnan

Particle and Astrophysics
Radboud University
Nijmegen, the Netherlands

July 2, 2025

Abstract

Extreme Mass Ratio Inspirals (EMRIs) will be important gravitational wave (GW) sources for the future LISA mission. A good theoretical understanding of these EMRIs is crucial for constructing correct waveforms. This thesis utilizes a theoretical framework that is based on black hole perturbation theory, to study tidal resonances in EMRIs, with a specific focus on the dynamic case. In doing so, this thesis aims to correctly calculate the jumps in the orbital constants of motion induced by a tidal resonance, for the most relevant resonance number combinations (n, k, m, s).

Our investigation resulted in two key results. First, it validates the "two-for-one deal", which is a relation that connects the tidal jumps in the Carter constant Q and the axial angular momentum L_z. The relation was shown to be accurate for stationary cases by previous work. We extend this work by expanding the analysis of the relation to more resonances and showing its accuracy in the dynamic case. Second, the influence of the perturber's orbital frequency Ω_{td} on the tidal jump calculations is analyzed, resulting in a predictable quadratic relationship. This thesis also focuses on determining the most relevant resonance number combinations (n, k, m, s), resulting in non-zero tidal jumps. In doing so, we find that a dynamic perturber can undergo multiple tidal jumps corresponding to one resonance number combination and some dynamic resonances can be excited even when no corresponding stationary resonance exists.

These findings are a step towards correctly interpreting the future data from LISA, as the next step for this research will be to complete the list of relevant tidal jumps and implement them into the Fast EMRI Waveform (FEW) python package.

Contents

1 Introduction

1.1 Gravitational waves

Gravitational waves (GWs) are ripples in spacetime, caused by highly energetic astrophysical events such as inspiraling black holes or rotating neutron stars. For roughly a decade now, since the first direct detection in 2015, we have been able to observe these GWs using so-called ground-based interferometers such as LIGO, Virgo and KAGRA (LVK) [1]. These detections marked the beginning of a new era in astrophysics, often referred to as gravitational wave astronomy. They have enabled us to observe the universe in a way not before possible, offering a complementary view to electromagnetic observations. This is because GWs interact only weakly with matter, but not nearly as much as EM waves do. Thus, they travel through the Universe nearly untouched, carrying valuable information about their sources. By observing these GWs, we can study extreme environments that were once purely theoretical and unobservable. Nonetheless, GWs are very weak compared to EM signals, making them much more difficult to detect.

In the next decade, gravitational wave astronomy will be complemented by data from space-based detectors such as the Laser Interferometer Space Antenna (LISA) [2, 3]. LISA will be sensitive to lower-frequency GWs than ground-based detectors, enabling us to observe sources that are currently inaccessible. One of the most exciting and scientifically rewarding classes of these sources that LISA is likely to observe will be Extreme Mass Ratio Inspirals (EMRIs). These are systems in which a stellar-mass compact object, say a black hole or neutron star, spirals into a supermassive black hole.

The detection of gravitational waves is based on a method known as matched filtering [4], where the observed signal is compared to a set of theoretical waveforms or "templates" that predict the signal based on the source's dynamics. Having physically realistic templates is crucial for detection purposes and for the extraction of physical information. If we do not have good waveforms, we cannot obtain the physical information about the source or the information can be unreliable. This becomes especially challenging in LISA, as its high sensitivity will detect many overlapping signals simultaneously. Inaccurate waveforms may lead to mistakes in the source identification, or even failing to detect weaker signals altogether due to the noise in the signal.

Therefore, highly accurate and computationally manageable waveform models are very important for the success of space-based GW astronomy. This thesis contributes to this effort by focusing on the theoretical modeling of EMRIs.

1.2 Extreme Mass Ratio Inspiral

An Extreme Mass Ratio Inspiral (EMRI) is a binary consisting of a compact stellar-mass object, like a black hole, neutron star, or white dwarf, gradually inspiraling into a much larger black hole, typically with a mass in the range of $10^5 - 10^7$ $M_\odot$[5]. The two objects' mass ratio is extreme, typically of the order of $10^{-5} - 10^{-7}$. Unlike comparable-mass binaries, EMRIs evolve over much longer durations within LISA's observable frequency band, taking 10^5–10^6 orbits in this band before their final plunge [6].

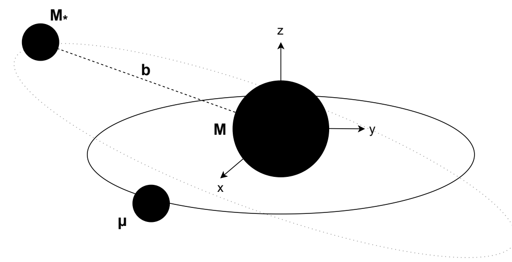

Figure 1: *An EMRI, consisting of a larger BH denoted by M and a smaller BH denoted by μ. The EMRI is perturbed by a third mass, denoted by M_* which we call the "tidal perturber", and lies at a distance b.*

As can be seen in figure 1, we will denote the mass of the tidal perturber as M_*, that of the central BH of the EMRI as M and its smaller mass as μ. The distance between the central BH and the tidal perturber will be denoted by b. The ratio of the smaller mass and the larger mass, also called the smallness parameter, is given by $\eta = \mu/M$.
The gravitational wave emission of EMRIs is characterized by highly complex waveforms. Unfortunately, the signals are typically weak, and very accurate waveform templates, together with long integration times, must be used to detect and analyze them via matched filtering. LISA's low-frequency sensitivity to gravitational waves makes it uniquely suited for the detection of these sources and at least a few hundred EMRIs are predicted to be observed by the LISA mission during its operation [7].

Due to their high mass ratio, EMRIs are studied in the context of black hole perturbation theory. In the limit when $\eta \to 0$, the smaller BH can be viewed as a test particle traveling through the background spacetime of the massive central BH. Thus, at leading order it will follow a geodesic in the Kerr spacetime. At the next order in η, the mass of the second BH leads to a contribution we call the "self-force". This force accounts for the object's own gravitational field and its backreaction on the motion, leading to a gradual inspiral.

More complex dynamics arise when additional perturbations, such as tidal fields of a third body or internal structures of the inspiraling body, are added. These perturbations can lead to tidal resonances, significantly altering the orbital constants of motion on relatively short timescales. Proper modeling of these effects is extremely crucial in order to extract reliable physical information from EMRI observations.

1.3 Report structure

This thesis expands a theoretical framework that is used to study the tidal effects on EMRIs, which is based on black hole perturbation theory and Post-Newtonian (PN) expansions. This framework is then used to calculate the so-called "tidal jump" for various relevant resonances and dynamically different variants of an EMRI, such as the prograde, retrograde, stationary and dynamic situations. The preceding introduction has given some necessary background for the following chapters. In chapter 2, the underlying theory of the research will be further explained until the level of research that was done. In chapter 3 we will present one of the two key findings from this thesis, which will concern the two-for-one deal. We will introduce and derive this relation and subsequently show its validity in both the stationary and dynamic case. In chapter 4, we will present the second main topic of this thesis, the influence of Ω_{td} on the tidal jump calculations. This will include an introduction of the relevant equations and a review of the results. Furthermore, this section will discuss some additional challenges that arise due to the effect of Ω_{td}. Finally, chapter 5 will present a discussion of the main findings and corresponding limitations of this study. We will also show some logical next steps to continue this research towards its end goal, beyond the scope of this report. This will be to implement the calculated tidal jumps in the Fast EMRI Waveform (FEW) Python package, which is part of the Black Hole Perturbation Toolkit (BHPT) [8]. Such that we can construct physically correct waveforms for EMRIs affected by tidal perturbers and accurately interpret the future data from LISA.

2 Theory

2.1 Self force and Tidal resonance

The dynamics of the smaller compact object in an EMRI can be described by black hole perturbation theory. To zeroth order, the object follows a geodesic in the Kerr spacetime, which we can characterize by three frequencies $(\omega_r, \omega_\theta, \omega_\phi)$ corresponding to radial, polar, and azimuthal motions, respectively. To expand this to first order, we use the so-called "action-angle formalism" [9]. Because of the integrability of the geodesic equations in Kerr, meaning there exists one integral of motion for each degree of freedom, we can introduce a set of "action-angle" variables. The "action" variables $\boldsymbol{J} = (J_r, J_\theta, J_\phi)$ are a function of the constants of motion. Namely, the orbital energy $E = -u_t$ in units of μ, the z component of the angular momentum $L_z = u_\phi$ in units of μM and the carter constant $Q = u_\theta^2 + \cos^2\theta(a^2(1-E^2) + (\frac{L_z}{\sin\theta})^2)$ in units of $\mu^2 M^2$, where u^α is the four-velocity of the smaller compact object in the EMRI, u_α is the corresponding covariant vector and $a = \frac{J}{M}$ is a spin parameter. Together, these uniquely define the shape of the orbit. The "angle" variables q_i parametrize the orbit, specifying the exact position of the object along its trajectory [10]. These q_i relate the orbital frequencies to the actions $\boldsymbol{J}$, via the orbital frequencies ω_i, since $\frac{dq_i}{d\tau} = \omega_i(J)$. The equations of motion are then expanded in the smallness parameter η, and a factor ϵ, determining the strength of the tidal field, given by [11]:

$$\epsilon = \frac{M_* M^2}{b^3}. \tag{1}$$

After expansion, we see that the change in the angle variables and the action variables can be written as

$$\frac{dq_i}{d\tau} = \omega_i(\boldsymbol{J}) + \epsilon g^{(1)}_{i,td}(q_r, q_\theta, q_\phi, \boldsymbol{J}) + \eta g^{(1)}_{i,sf}(q_r, q_\theta, \boldsymbol{J}) + \mathcal{O}(\eta^2, \epsilon^2, \eta\epsilon) \tag{2}$$

$$\frac{dJ_i}{d\tau} = \eta G^{(1)}_{i,sf}(q_r, q_\theta, q_\phi) + \epsilon G^{(1)}_{i,td}(q_r, q_\theta, q_\phi, \boldsymbol{J}) + \mathcal{O}(\eta^2, \epsilon^2, \eta\epsilon). \tag{3}$$

Clearly separating the self force, denoted by the sf subscript, and the tidal force, denoted by the *td* subscript. Utilizing this separation, this thesis will focus its research on the tidal force and in doing so, omit the self force contribution in equation (3).

Specifically, we will focus on the so-called "tidal resonance", by dropping the *td* subscript in equation (3). Then, according to an adiabatic approximation, we find that to lowest order we can write this equation as [12]

$$\frac{dJ_i}{d\tau} \approx \epsilon \left\langle G_i^{(i)}(q_r, q_\theta, q_\phi, \boldsymbol{J}) \right\rangle, \tag{4}$$

where the angular brackets $\langle \quad \rangle$ denote the phase space average over the 3-torus spanned by the angles. This simplification is allowed because the EMRI system evolves adiabatically in this regime. The so-called radiation reaction time T_{rad} is much larger than the orbital time T_{orb}, thus $T_{orb}/T_{rad} \sim \mu/M \ll 1$, making the adiabatic approximation a viable simplification [13]. This tidal force can now be decomposed and written as a Fourier series, such that

$$G_i^{(1)}(q_r, q_\theta, q_\phi, \boldsymbol{J}) = \sum_{n,k,m} G_{i,nkm}^{(1)}(\boldsymbol{J}) e^{i(nq_r + kq_\theta + mq_\phi)}. \tag{5}$$

For generic (ergodic) orbits the phase factor oscillates rapidly and averages out to zero over many cycles. So ordinary n, k, m modes produce no long-term change in the actions $\boldsymbol{J_i}$. However, if at some moment the frequencies satisfy

$$n\omega_r + k\omega_\theta + m\omega_\phi = 0, \tag{6}$$

then the exponential becomes equal to one. This results in a nonzero change in $\boldsymbol{J_i}$, meaning a tidal resonance has occurred [10]. Here, n, k, m are integers called the resonance numbers and they denote a specific resonance. These jumps in $\boldsymbol{J_i}$, and thus in the constants of motion (E, L_z, Q), significantly change the dynamics and therefore, leave measurable imprints on the gravitational wave signal.

2.2 Different Scenarios

Finally, we will describe different scenarios in which the tidal resonance can occur in an EMRI. All of these scenarios have distinct effects on the calculation of the jump sizes and thus should be distinguished from each other.

Firstly, we can make a distinction when comparing the orbital motion of the smaller mass of the EMRI and the rotation of the central BH, in other words its spin. When these two are in the same direction, we call this a prograde motion, as seen in figure 2a. When these are in the opposite direction of each other, we call this a retrograde motion, as seen in figure 2b. This distinction is important when determining which combination of resonance numbers n, k, m are relevant. For prograde motion, all frequencies are positive, whereas for retrograde motion, ω_ϕ is (by definition) negative. Looking at the resonance condition from equation

(6), we see that a negative ω_ϕ will change for which n, k, m values the resonance condition is satisfied.

(a) *Prograde* *(b)* *Retrograde*

Figure 2: *Prograde and retrograde motion of an EMRI. In the case of prograde motion, the smaller mass of the EMRI μ is rotating in the* <u>*same direction*</u> *as the spin of the central BH. In the case of retrograde motion, it is rotating in the* <u>*opposite direction*</u> *as the spin of the central BH.*

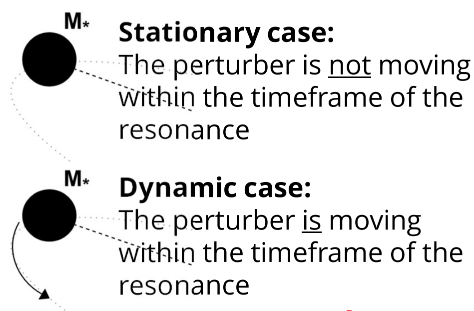

Figure 3: *Difference between the stationary case and the dynamic case.*

Secondly, we make the distinction between a stationary perturber and a dynamic perturber as explained here in figure 3. This means that within the duration of the resonance, the perturber will either be stationary or will be moving in its trajectory around the EMRI. In the dynamic case, we allow the perturber to move in a circular orbit. In both cases, the perturber may have an arbitrary inclination angle.

Intuitively, we can already see that the stationary case will be much simpler to describe mathematically. Specifically, the resonance condition from equation (6) differs in the dynamic case. This resonance condition is now also dependent on the orbital frequency of the perturber, Ω_{td}, which was zero in the stationary case. Thus the resonance condition is now given by

$$n\omega_r + k\omega_\theta + m\omega_\phi + s\Omega_{\text{td}} = 0\,. \tag{7}$$

As a result, the Fourier decomposition of the jump amplitude from equation (5) also changes, such that

$$G_i^{(1)}(q_r, q_\theta, q_\phi, Q_{td}, \boldsymbol{J}) = \sum_{n,k,m,s} G_{i,nkms}^{(1)}(\boldsymbol{J}) e^{i(nq_r + kq_\theta + mq_\phi + sQ_{td})}, \tag{8}$$

where Q_{td} is defined such that $\Omega_{\text{td}} = \frac{dQ_{\text{td}}}{dt}$.

Finally, we provide an alternative way of describing the shape of the orbit of the smaller mass in an EMRI, with mass μ. As mentioned in section 2.1, the constants of motion (E, L_z, Q) uniquely describe the shape of the orbit and together with the mass and spin of the central BH, they uniquely describe the full system. Alternatively, we can use the parameters (a, M) and variables (p, e, x) to fully describe this system and its dynamics. Here, $a = \frac{J}{M}$ is a spin parameter, p is the semi-latus rectum, e is the orbital eccentricity and $x = \cos(I)$, where I is the orbital inclination. These variables are much more convenient to use because they are bounded: $0 < a < 1$, $0 < e < 1$, $-1 \leq x \leq 1$ and the semi-latus rectum has its lower limit at the so-called "separatrix", $p > p_s$. The explicit relations between the description in terms of a, p, e and x and the description in terms of E, L_z and Q can be found in [14].

2.3 Calculating the jump

The aim of this section will be to explain how we calculate the jump sizes in the orbital constants of motion induced by a tidal resonance. We will split this problem into multiple parts, briefly going over the most important elements in this derivation. The complete framework for studying these stationary and dynamic tidal resonances has been developed in previous work [10, 15, 16]. The following sections provide the necessary background for a working understanding of the Mathematica code that was used in these calculations. To calculate the jump, we will need to calculate the evolution of the orbital constants of motion $(\frac{dE}{d\lambda}, \frac{dL_z}{d\lambda}, \frac{dQ}{d\lambda})$, since they will be the integrands needed to ultimately calculate the jump sizes in section 2.3.3 as can be seen in equation (28).

First, we will find an expression for the metric perturbation $h_{\mu\nu}$ in section 2.3.1. We will need this to find the acceleration a^μ, which is needed in order to calculate the evolution of the orbital constants of motion.

Second, we will study the Kerr geodesics in section 2.3.2 in order to find the four-velocity u^α, which we will also need to calculate the evolution of the orbital constants of motion. On top of this, this section will define the orbital frequencies $(\omega_r, \omega_\theta, \omega_\phi)$. This will be essential in solving the resonance condition as stated in equation (7) in section 2.2.

Finally, we will combine these sections to show we can find the jump sizes in section 2.3.3.

2.3.1 Perturbation theory

We will now derive an expression for the metric perturbation $h_{\mu\nu}$ induced by a tidal perturber, and the acceleration induced by this metric perturbation, which we will need in section 2.3.3. The background to this perturbation will be a rotating BH. However, we will simplify the calculations by neglecting the central BH's spin at this stage. Thus, we use the Schwarzschild metric as background instead of a Kerr metric when calculating $h_{\mu\nu}$. Previous work has shown that making this approximation will only slightly reduce the accuracy of the results, but significantly improves computational efficiency. In particular, the results of these different approaches only differ by 0.1% generally. (They differ by 1% at most for highly eccentric orbits). While the calculation takes 15 times longer using the Kerr metric when compared to using the Schwarzwild metric [17].

The complete metric will be given by

$$\tilde{g}_{\mu\nu} = g_{\mu\nu} + h_{\mu\nu}, \tag{9}$$

where $g_{\mu\nu}$ is the Schwarzschild metric and $h_{\mu\nu}$ is the perturbation we are looking for. This perturbation is most easily found by expressing it in tidal quadrupole moments $\mathcal{E}_{ab}(t)$ and $\mathcal{B}_{ab}(t)$, which are the even parity gravitoelectric moments and the odd parity gravitomagnetic moments, respectively. The even parity moments arise from the mere presence of the perturber, while the odd parity moments are caused by the dynamics of the perturber and are thus proportional to its orbital velocity. Hence, in the stationary case, where the perturber's orbital velocity is zero throughout the duration of the resonance, the odd parity gravitomagnetic moments $\mathcal{B}_{ab}$ equal zero. The metric in terms of tidal moments can be written as

$$\begin{aligned}
&\tilde{g}_{tt} = -f + r^2 e^q_{tt}\mathcal{E}^q, \\
&\tilde{g}_{tr} = 0 \\
&\tilde{g}_{rr} = f^{-1} + r^2 e^q_{rr}\mathcal{E}^q \\
&\tilde{g}_{tA} = r^3 b^q_t \mathcal{B}^q_A \\
&\tilde{g}_{rA} = 0 \\
&\tilde{g}_{AB} = r^2\Omega_{AB}(1 + r^2 e^q \mathcal{E}^q)
\end{aligned} \tag{10}$$

where $f = 1 - \frac{2M}{r}$. We only take into account the quadrupole moments and not the higher-order moments such as octupole and hexadecapole moments, since they are suppressed in the so-called "small-tide approximation" [18]. That is, when $M \ll \mathcal{R} \sim \sqrt{\frac{b^3}{M+M_*}}$. Here, $\mathcal{R}$ is the radius of curvature of the external spacetime and represents the characteristic length scale over which the tidal forces, generated by the distant perturber (with mass M_* at distance b), vary significantly. The "external spacetime" refers to the gravitational field induced by the tidal perturber, as experienced at the location of the secondary BH in the EMRI, denoted by μ. The condition $M \ll \mathcal{R}$ ensures that the tidal interaction is weak. This is crucial because it allows us to describe the secondary BH as an object responding to a gravitational field induced by the perturber. If, on the other hand, M were comparable to $\mathcal{R}$, the secondary BH itself would significantly distort the very gravitational field it is supposed to be reacting to, and no clear distinction could be made between the secondary BH's intrinsic spacetime and the external spacetime.

All that remains in order to express the metric perturbation $h_{\mu\nu}$ in terms of tidal moments are spherical harmonics. Specifically, scalar spherical harmonics $Y^{lm}(\theta^A)$ for the even parity and vectorial harmonics $X_A^{2m}(\theta^A)$ for the odd parity. These tidal moments and spherical harmonics together construct the so-called tidal potentials $\mathcal{E}^q$ and $\mathcal{B}_A^q$, which is what our metric perturbation depends on, and they look like [19]

$$\mathcal{E}^q(t,\theta^A) = \sum_{-2\leq m\leq 2} \mathcal{E}_m^q(t) Y^{2m}(\theta^A) \tag{11}$$

and

$$\mathcal{B}_A^q(t,\theta^A) = \frac{1}{2}\sum_{-2\leq m\leq 2} \mathcal{B}_m^q(t) X_A^{2m}(\theta^A). \tag{12}$$

Here, we only account for the quadrupole moments ($l=2$), as explained previously. The analytical expressions for the spherical harmonics $Y^{2m}(\theta^A)$ and $X_A^{2m}(\theta^A)$ can be found in table 1 and table 2 of [17]. Similarly, the relations between $\mathcal{E}_m^q$ and $\mathcal{E}_{ab}$ and those between $\mathcal{B}_m^q$ and $\mathcal{B}_{ab}$ can be found in table 1 and table 2 of [17].

In order to now find the correct analytical expression for the tidal moments, $\mathcal{E}_m^q(t)$ and $\mathcal{B}_m^q(t)$, we will use a method called metric matching [19]. Effectively, this means comparing the metric as written in terms of the tidal moments, as shows in equation (10), with a Post-Newtonian (PN) metric of the Schwarzschild BH. This PN metric of the Schwarzschild BH is given by

$$\begin{aligned}
\tilde{g}_{tt} &= -1 + 2U + 2(\Psi - U^2) + 2\mathrm{PN} \\
\tilde{g}_{ta} &= -4U_a + 2\mathrm{PN} \\
\tilde{g}_{ab} &= (1+2U)\delta_{ab} + 2\mathrm{PN}
\end{aligned} \tag{13}$$

where U is a Newtonian potential, Ψ is a PN potential, U_a is a vector potential and $+2PN$ denotes any second order Post-Newtonian contributions [20]. After metric matching, the details of which can be found in [19, 21], we find that the electric and magnetic quadropole moments, describing the influence of a compact object with mass M_* at a distance b with orbital frequency Ω_{td}, can be written as

$$\mathcal{E}_{ab}(t) = -3\frac{M_*}{b^3} n_{\langle a} n_{b\rangle} + 1\mathrm{PN}, \tag{14}$$

and

$$\mathcal{B}_{ab}(t) = -6\frac{M_* u}{b^3} n_{\langle a} l_{b\rangle} + 1\mathrm{PN}, \tag{15}$$

where

$$\begin{aligned} n_{\langle a}l_{b\rangle} &= \tfrac{1}{2}(n_a l_b + l_a n_b) - \tfrac{1}{3}\delta_{ab}n^c l_c\ , \\ n_a &= \Big(-\cos(\Omega_{\rm td}t), \sin(\Omega_{\rm td}t), 0\Big) \text{ and} \\ \lambda_a &= \Big(\sin\left(\Omega_{\rm td}t\right), -\cos\left(\Omega_{\rm td}t\right), 0\Big). \end{aligned} \tag{16}$$

Combining these equations, we find an analytical expression for the metric perturbation $h_{\mu\nu}$. Finally, we can use this to calculate the induced acceleration as a function of this perturbation $h_{\mu\nu}$, the background metric $g_{\mu\nu}$ and the four-velocity u^α [10], which are related in the following way:

$$a^\alpha = -\frac{1}{2}\left(g^{\alpha\beta} + u^\alpha u^\beta\right)\left(2\nabla_\rho h_{\beta\lambda} - \nabla_\beta h_{\lambda\rho}\right)u^\lambda u^\rho + \mathcal{O}(h^2), \tag{17}$$

with ∇_α being the covariant derivative compatible with the background metric.

2.3.2 Kerr Geodesics

To understand the perturbed motion of the smaller mass in the EMRI, we first examine its unperturbed, geodesic motion in the Kerr spacetime of the central BH. This section provides the geodesic equations that describe this motion and gives the key quantities, the four-velocity components u^α and the fundamental orbital frequencies ω_i. These will be important for sections 2.3.3 and 2.3.4 respectively. There, we will use them to calculate the acceleration a^α, needed to find the jump in the orbital constants of motion, and understand the fundamental orbital frequencies ω_i, needed for the resonance condition of equation (7) and its application.

We will utilize the extremely small mass ratio η and describe the dynamics of the secondary mass of the EMRI by the geodesic equations in Kerr spacetime. Combining the Kerr metric with the constants of motion (E, L_z, Q), and using Boyer-Lindquist coordinates (t, r, θ, ϕ), we find that the geodesic equations are given by four ordinary differential equations [22, 23, 24]. We use Mino time λ to parametrize these equations, such that the radial and polar contributions can be separated clearly. Mino time is related to proper time τ by $d\tau = \Sigma d\lambda$(, where $\Sigma = r^2 + a^2\cos^2\theta$). These geodesic equations take the following form:

$$\begin{aligned} \tfrac{dt}{d\lambda} &= T_r(r) + T_\theta(\cos\theta) + aL_z, \\ \left(\tfrac{dr}{d\lambda}\right)^2 &= R(r), \\ \left(\tfrac{d\theta}{d\lambda}\right)^2 &= \Theta(\theta), \\ \tfrac{d\phi}{d\lambda} &= \Phi_r(r) + \Phi_\theta(\cos\theta) - aE, \end{aligned} \tag{18}$$

where

$$\begin{aligned}
&R(r) = (E(r^2+a^2) - aL_z)^2 - \Delta(r^2 + (L_z - aE)^2 + Q),\\
&T_r(r) = \tfrac{r^2+a^2}{\Delta}(E(r^2+a^2) - aL_z),\\
&\Phi_r(r) = \tfrac{a}{\Delta}(E(r^2+a^2) - aL_z),\\
&\Theta(\theta) = Q - L_z^2 \cot^2\theta - a^2(1-E^2)\cos^2\theta,\\
&T_\theta(\cos\theta) = a^2 E(\cos^2\theta - 1),\\
&\Phi_\theta(\cos\theta) = \tfrac{L_z}{1-\cos^2\theta}.
\end{aligned} \tag{19}$$

From the equations of motion in equation (18), we can read of the $\frac{dx^\alpha}{d\lambda}$ needed in order to find the four-velocity, which is then given by

$$u^\alpha = \frac{dx^\alpha}{d\tau} = \frac{dx^\alpha}{d\lambda}\frac{d\lambda}{d\tau} = \frac{1}{\Sigma}\frac{dx^\alpha}{d\lambda}. \tag{20}$$

Solving these differential equations, results in finding periodic functions for $r(\lambda)$ and $\theta(\lambda)$ and non-periodic functions for $t(\lambda)$ and $\phi(\lambda)$, which can be written as

$$\begin{aligned}
t(\lambda) &= t_0 + \Gamma_t\lambda + t_\lambda^{(r)} + t_\lambda^{(\theta)},\\
\phi(\lambda) &= \phi_0 + \Gamma_\phi\lambda + \phi_\lambda^{(r)} + \phi_\lambda^{(\theta)}.
\end{aligned} \tag{21}$$

In this equation, t_0 and λ_0 give the initial conditions, $t_\lambda^{(r)}$, $t_\lambda^{(\theta)}$, $\phi_\lambda^{(r)}$ and $\phi_\lambda^{(\theta)}$ give the oscillatory dependency and most importantly, Γ_t and Γ_ϕ are the so-called temporal and azimuthal Mino-time frequencies [25], which can also be written as

$$\begin{aligned}
\Gamma_t &= \langle T_r(r)\rangle_\lambda + \langle T_\theta(\cos\theta)\rangle_\lambda + aL_z\\
\Gamma_\phi &= \langle \Phi_r(r)\rangle_\lambda + \langle \Phi_\theta(\cos\theta)\rangle_\lambda - aE.
\end{aligned} \tag{22}$$

In equation (22), the angular brackets $\langle\ \ \rangle$ denote a time averaging with respect to λ [22]. The periodic functions for $r(\lambda)$ and $\theta(\lambda)$ will have periods given by

$$\begin{aligned}
\Lambda_r &= 2\int_{r_p}^{r_a} \tfrac{dr}{\sqrt{R(r)}},\\
\Lambda_\theta &= 4\int_{\theta_{min}}^{\frac{\pi}{2}} \tfrac{d\theta}{\sqrt{\Theta(\theta)}}.
\end{aligned} \tag{23}$$

In which r_p is the periapsis, r_a is the apoapsis and θ_{min} is the minimum value of θ. Consequently, the radial and polar Mino-time frequencies are then given by their corresponding periods

$$\Gamma_{r,\theta} = \frac{2\pi}{\Lambda_{r,\theta}}. \tag{24}$$

Finally, knowing how to express these Mino-time frequencies, we can find the orbital frequencies in the following way

$$\omega_{r,\theta,\phi} = \frac{\Gamma_{r,\theta,\phi}}{\Gamma_t}. \tag{25}$$

2.3.3 Jumps in orbital constants of motion

The change in the orbital constants of motion $\boldsymbol{J}$, induced by the tidal resonance, can be well approximated by [26]

$$\begin{aligned}\Delta J_i &= \epsilon \int_{-\infty}^{\infty} G_i^{(1)}(q_r, q_\theta, q_\phi, \boldsymbol{J}) d\tau \\ &= \frac{\epsilon}{\eta^{1/2}} \sum_s \sqrt{\frac{2\pi}{|\Gamma s|}} \exp\left[\mathrm{sgn}(\Gamma s)\frac{i\pi}{4} + is\chi\right] G^{(1)}_{i,smsksn}\,,\end{aligned} \tag{26}$$

where s is a non-zero integer, $\Gamma := m\dot{\omega}_{\phi 0} + k\dot{\omega}_{\theta 0} + n\dot{\omega}_{r0}$ and $\chi := mq_{\phi 0} + kq_{\theta 0} + nq_{r0}$. The dots above the omegas denote a derivative with respect to proper time evaluated at the time of resonance τ_0.
This equation can be divided into three components and thus written as

$$\Delta J_i = \text{“resonance duration”} \times \exp(\text{“phase”}) \times \text{“jump amplitude”}. \tag{27}$$

The resonance duration is the part given by $\sqrt{\frac{2\pi}{|\Gamma s|}}$ and the phase is given by the exponent $\mathrm{sgn}(\Gamma s)\frac{i\pi}{4} + is\chi$. This thesis specifically focuses on the jump amplitude, which is given by the Fourier coefficients $G^{(1)}_{i,smsksn}$. While equation (26) describes the jump in terms of action variables J_i and their corresponding Fourier coefficients $G^{(1)}_{i,smsksn}$, we are ultimately interested in the jumps in orbital constants of motion $\mathcal{C}$ (namely, E, L_z, Q). Since the action variables are functions of these orbital constants (as discussed in section 2.1), a jump in J_i directly translates to jumps in $\mathcal{C}$. Therefore, to determine the amplitudes of these jumps in $\mathcal{C}$, we calculate the Fourier coefficients for the rates of change of E, L_z, and Q. We can find these Fourier coefficients using the following averaging integrals given by

$$\left\langle \frac{d\mathcal{C}}{dt} \right\rangle\bigg|_{nkm} = \frac{1}{\Gamma_t (2\pi)^3} \int_0^{2\pi} dq_r \int_0^{2\pi} dq_\theta \int_0^{2\pi} dq_\phi \frac{d\mathcal{C}}{d\lambda} e^{-i(nq_r + kq_\theta + mq_\phi)}, \tag{28}$$

where $\frac{d\mathcal{C}}{d\lambda}$ are the $\frac{dE}{d\lambda}$, $\frac{dL_z}{d\lambda}$ and $\frac{dQ}{d\lambda}$.
It is important to consider how the orbital energy E behaves. With a stationary tidal perturber, the tidal field does not change over time. This means that $\frac{dE}{dt} = 0$ from this interaction. On the other hand, for a dynamic perturber, the tidal field is time-dependent. While this allows for some energy exchange ($\frac{dE}{dt}$ is not exactly zero), previous work has found that no jump in the orbital energy E is induced, even in the dynamic case [17]. Thus, in the re-

mainder of this thesis we focus on the jumps in L_z and Q.
In order to find these, we need the acceleration a^α which we found in section 2.3.1. Knowing a^α, we can write them as [20]

$$\begin{aligned} \tfrac{dL_z}{d\tau} &= a_\phi, \\ \tfrac{dQ}{d\tau} &= 2u_\theta a_\theta - 2a^2\cos^2\theta u_t a_t + 2\cot^2\theta u_\phi a_\phi. \end{aligned} \tag{29}$$

Finally, in equation (29) we used proper time τ instead of Mino time λ, by using the relation $d\tau = \Sigma\, d\lambda$.

2.3.4 Selection rules for resonance numbers

In order to satisfy the resonance condition in equation (7), we need to find a combination of n, k, m, s values for which we can find a resonance. Not all combinations of these integers will lead to a significant jump in the orbital constants of motion. In order to determine the relevant combinations, we make use of multiple so-called "selection rules" and characteristics of the resonance condition. This section will briefly cover these selection rules and narrow down the amount of n, k, m, s combinations that will be relevant both in the stationary case and in the dynamic case.

First, we focus on the stationary tidal perturber, for which the resonance condition simplifies as the perturber's own orbital frequency Ω_{td} is zero, meaning the resonance number s is not part of the condition. When the perturber is located in the equatorial plane of the central BH, only resonances with an even integer for the polar resonance number k (i.e., k =even) contribute to changes in the axial component of the angular momentum, L_z [27]. Consequently, this rule also applies to jumps in Q, as long as $m \neq 0$. This is due to the "two-for-one deal", which relates jumps in L_z and the Carter constant Q and we will explain this further in chapter 3.
For a more general case where the stationary perturber is not confined to the equatorial plane, the following selection rule applies: a jump is induced in L_z only if the sum of the polar and azimuthal resonance numbers, $k + m$, is even. If $k + m$ is odd, the resonance does not lead to a change in these constants of motion.

When considering a dynamic tidal perturber, the perturber's orbital frequency Ω_{td} is non-zero, and the resonance number s associated with this frequency plays a crucial role. The most general selection rule for a dynamic perturber (which may also be on an inclined orbit relative to the EMRI's equatorial plane) states that a jump in L_z and Q is induced only if the sum $k + m + s$ is an even integer. Resonances where $k + m + s$ is odd will not cause a change in L_z or Q [27]. This general rule naturally reduces to the stationary case rules. If the perturber is stationary $(s = 0)$, the rule becomes $k + m$ =even. If the stationary perturber is also on the equatorial plane (where only $m = 0, 2$ are typically relevant for the electric quadrupole contribution), this further simplifies, consistent with k =even.

Beyond applying the main selection rules that tell us which types of resonances can physically occur, we take a few more practical steps to narrow down the list of specific resonance number combinations we want to study.
First, when we initially list possible integer combinations for n, k, m (and s for the dynamic case), we make sure to handle how positive and negative numbers are treated. We do not need to consider combinations where all the contributions of the resonance condition, in equation (7), are positive and also separately where they are all negative. Because then these will never fulfill the resonance condition, since the total must equal zero. For prograde motion, this means n, k, m, s cannot all be the same sign, since then the orbital frequencies are all positive. For retrograde motion however, the ω_ϕ is by definition negative. Thus this means we cannot have n, k, s positive and m negative, or vice versa. On top of this, a resonance defined by a particular set of integers (e.g., (1, 2, -1)) is equivalent to the resonance defined by the set with all signs inverted (e.g., (-1, -2, 1)). Thus, we use a convention to make sure each resonance is considered only once. We choose to always make the first number, n, positive. If n happens to be zero, then we make the next number, k, positive, and so on for m and s.
Another important step is to concentrate on the "low-order" or fundamental resonances. These are the combinations made with smaller integer values. If we find a basic resonance, like (1, 2, -1), then other resonances that are just multiples of it do not have as strong an effect and are called subdominant [28], for example with (2, 4, -2) where all the numbers are just doubled. Because of this, we filter out these "higher-order multiples." This means that if we have picked a specific combination to study, we then remove any other combinations that are just that lowest-order combination multiplied by two, or by three, and so on. Finally, we focus on the resonance number combinations for which the integers are limited, so specifically $(n, k) \leq 4$ and $(m, s) \leq 2$. Here, we limited (n, k) in order to focus on the lower-order resonances, i.e. those with the most impact.[1] We limited the values for (m, s) because we restrict our analysis to the quadrupole $(l = 2)$ field by using the small-tide approximation [18].

[1]The choice of these limits was supported by calculating several jumps with $n = 5$ and $n = 6$. Specifically, we observed for prograde resonances with combinations $(5, -4, 2)$, $(5, -1, -1)$, $(6, -3, -1)$ and $(6, 0, -2)$ and for retrograde resonances with combinations $(5, -4, 0)$, $(5, -3, 1)$, $(6, -1, 1)$ and $(6, -4, -2)$ that the jumps are indeed 3 orders of magnitude smaller in those cases, compared to the typical jump sizes for $n \leq 4$.

By taking these extra steps after the main selection rules, we end up with a cleaner list. It contains the unique resonance combinations that are most likely to cause noticeable changes in the EMRI's orbit, making our detailed calculations more targeted and efficient. We determined this cleaner list using a Mathematica code. Both the methods with which we determined this and the results are shown in appendix B.

Looking at these results, we observe that we have 88 relevant (n, k, m, s) combinations in the stationary case and 708 in the dynamic case. This clearly shows that the more complex dynamic case will require more computations to fully analyze and understand. However, this list can be made even shorter by focusing on resonances that occur at a reasonably small value for the semi-latus rectum p. For example, when we further limit ourselves to the (n, k, m, s) combinations that results in a resonance with a value of $p \leq 100$, we are left with 24 resonance combinations for the stationary case and 316 for the dynamic case.

3 Two-for-one deal

In this section, we will explain one of the main interests of this thesis, the so-called two-for-one deal [29]. This "deal" describes a closed relation that relates the jump in the Carter constant Q with the jump in the axial component of the angular momentum L_z, by a prefactor that depends only on the resonance numbers n, k and m and the values of a, p, e and x. Thus, we see that these tidal jumps are in fact not independent. We can compute the change in one of them, given the other, by using this relation. Direct computation of these tidal jumps, as done in previous sections of this thesis, is computationally costly. Thus, having a good understanding of this relation will offer a drastic simplification for calculating accurate tidal jumps. In this section, we will show a derivation for this relation. In previous work [29], this relation has already been shown to give accurate results for three resonances, the (3,0,-2) resonance, the (3,-4,2) resonance and the (-3,1,1) resonance. This was done in the setting with a stationary perturber and for a limited number of initial conditions. We have extended this original analysis by investigating additional resonances, for various different initial conditions by also varying the parameters a, e and x. In addition, we will add to this work by showing that this relation also performs well for systems with dynamic perturbers.

3.1 Deriving the relation

This derivation, as done in [29], uses a Hamiltonian framework in action-angle variables, which is what we are familiar with from section 2.1. More background on this derivation can also be found in [30]. During this derivation, we do not take into account any effect from the mass of the smaller BH. The Carter constant Q is only a function of E, L_z and J_r. Since in this treatment, the same is true for J_θ, we can write

$$1 = \left(\frac{\partial Q}{\partial Q}\right)_{E,L_z} = \left(\frac{\partial Q}{\partial J_r}\right)_{E,L_z} \left(\frac{\partial J_r}{\partial Q}\right)_{E,L_z}, \tag{30}$$

$$0 = \left(\frac{\partial Q}{\partial L_z}\right)_{E,Q} = \left(\frac{\partial Q}{\partial J_r}\right)_{E,L_z} \left(\frac{\partial J_r}{\partial L_z}\right)_{E,Q} + \left(\frac{\partial Q}{\partial L_z}\right)_{E,J_r}. \tag{31}$$

Starting with the chain rule for the rate of change of the Carter constant Q with respect to proper time τ, we have

$$\frac{dQ}{d\tau} = \left(\frac{\partial Q}{\partial J_r}\right)_{E,L_z} \frac{dJ_r}{d\tau} + \left(\frac{\partial Q}{\partial L_z}\right)_{E,J_r} \frac{dL_z}{d\tau}. \tag{32}$$

From equation (31) we can write

$$\left(\frac{\partial Q}{\partial L_z}\right)_{E,J_r} = -\left(\frac{\partial Q}{\partial J_r}\right)_{E,L_z}\left(\frac{\partial J_r}{\partial L_z}\right)_{E,Q}. \tag{33}$$

Substituting this back into equation (32) yields

$$\frac{dQ}{d\tau} = \left(\frac{\partial Q}{\partial J_r}\right)_{E,L_z}\frac{dJ_r}{d\tau} - \left(\frac{\partial Q}{\partial J_r}\right)_{E,L_z}\left(\frac{\partial J_r}{\partial L_z}\right)_{E,Q}\frac{dL_z}{d\tau}. \tag{34}$$

The jumps in the action variables are proportional, specifically $dJ_r/d\tau = (n/m)dL_z/d\tau$. This is a direct result from equation 20 in [29] given that $J_\phi = L_z$ from equation 13 in [29]. Incorporating this proportionality, we get

$$\frac{dQ}{d\tau} = \left(\frac{\partial Q}{\partial J_r}\right)_{E,L_z}\left[\frac{n}{m} - \left(\frac{\partial J_r}{\partial L_z}\right)_{E,Q}\right]\frac{dL_z}{d\tau}. \tag{35}$$

Finally, using equation (30), which implies $\left(\frac{\partial Q}{\partial J_r}\right)_{E,L_z} = \left(\frac{\partial J_r}{\partial Q}\right)^{-1}_{E,L_z}$, we arrive at

$$\frac{dQ}{d\tau} = \left[\frac{n}{m} - \left(\frac{\partial J_r}{\partial L_z}\right)_{E,Q}\right]\left(\frac{\partial J_r}{\partial Q}\right)^{-1}_{E,L_z}\frac{dL_z}{d\tau}. \tag{36}$$

Relation (36) can be written more explicitly as

$$\frac{dQ}{d\tau} = \frac{\frac{\pi a k}{m}\sqrt{1-E^2}\,y_+ - 2L_z\left(K[(\frac{y_-}{y_+})^2] - \Pi[y_-^2,(\frac{y_-}{y_+})^2]\right)}{K[(\frac{y_-}{y_+})^2]}\frac{dL_z}{d\tau}, \tag{37}$$

where $K[m]$ and $\Pi[n,m]$ are the complete elliptic integrals of the first and third kind respectively. These are given by

$$K[m] \equiv \int_0^{\frac{\pi}{2}} \frac{d\phi}{\sqrt{1-m\sin^2\phi}} = \int_0^1 \frac{dx}{\sqrt{(1-x^2)(1-mx^2)}}, \tag{38}$$

$$\Pi[n,m] \equiv \int_0^{\frac{\pi}{2}} \frac{d\phi}{(1-n\sin^2\phi)\sqrt{1-m\sin^2\phi}} = \int_0^1 \frac{dx}{(1-nx^2)\sqrt{(1-x^2)(1-mx^2)}} \tag{39}$$

and $y_\pm$ are given by

$$y_\pm^2 = \frac{a^2(1-E^2)+L_z^2+Q \pm \sqrt{\left(a^2(1-E^2)+L_z^2+Q\right)^2 + 4a^2(E^2-1)Q}}{2a^2(1-E^2)}. \tag{40}$$

Because $Q > 0$ and $1 - E^2 > 0$, we can see that $y_+ > y_-$. These $y_\pm$ are defined as the values of $\cos^2\theta$ at the points where the potential $V_\theta = Q - \cos^2\theta \left[a^2(\mu^2 - E^2) + \frac{L_z^2}{\sin^2\theta}\right]$ is zero. Alternatively, we can write this potential as

$$V_\theta(\theta) = a^2(1 - E^2)\frac{(y_+^2 - \cos^2\theta)(y_-^2 - \cos^2\theta)}{\sin^2\theta}. \tag{41}$$

The relation in equation (37) is known as the “two-for-one deal” and will greatly reduce the computational costs of the tidal jump calculations.

3.2 Results

Now that we have established the derivation of the two-for-one deal relation, we will focus on applying it. As seen in previous work [29], this relation is shown to be accurate within the error of 0.01% for three different resonances (all with $n = 3$) for a stationary perturber. We will confirm these results by recreating them. During the derivation in section 3.1, the perturber was treated as stationary. Despite this, we will show that this relation still is accurate for the case with a dynamic perturber within the error of 0.03% in a similar case.

First, we will show the results for the stationary case. We compare the values of the jump size in Q as calculated using the method described in section 2.3.3, with the values for Q according to the two-for-one deal relation. We also look at the relative error, i.e. the absolute value of the relative difference between these two differently calculated values for the Carter constant Q divided by the directly calculated value for Q, which is given by

$$\text{Relative Error} = \frac{|Q_{\text{calculated}} - Q_{\text{two-for-one deal}}|}{Q_{\text{calculated}}}. \tag{42}$$

We start by looking at the resonance for $(n, k, m) = (3, 0, -2)$ in the stationary case, these results can be found in figure 4.

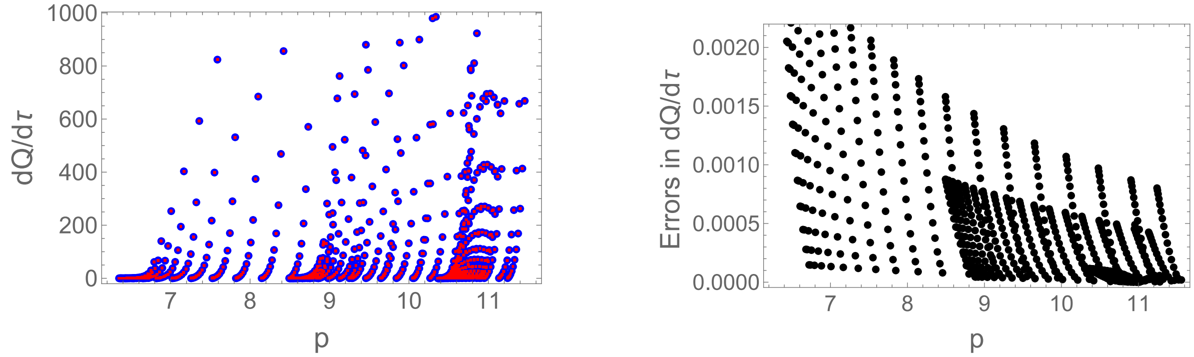

(a) ***(b)***

Figure 4: *Validation of the two-for-one deal for jumps in the Carter constant Q induced by a* ***stationary perturber*** *for the resonance number combination $(3, 0, -2)$. The left plot compares the values for the jump in Q as calculated using the two-for-one deal relation (denoted by the red blocks) and as calculated using the jump size calculations (denoted by the blue circles). The vertical axis shows the jump sizes and the horizontal axis shows the value of p for which the resonance occurs. On the right we plot the relative error for each set, which is given by the absolute value of the relative difference between the two value of the left plot.*

As can be seen, these results align nicely and this confirms the previous work of [29]. On the left of figure 4, we show a comparison of the values for the jump in Q as calculated using the two-for-one deal relation (denoted by the red blocks) and as calculated using the jump size calculations (denoted by the blue circles). On the right we show the relative errors, which are given by the absolute value of the relative difference between the two value of the left plot, as described in equation (42). Every pair of blue and red dots denotes a single input value for the parameters a, e and x, so every point in the plot depicts a different dynamical situation. Specifically, when we compare our results to the results from [29], we establish a similar accuracy. First, we fix the values of e and $x = \cos(I)$ to be 0.7 and 0.96 respectively, in order to fully recreate the conditions of the paper, while varying the values for the spin parameter a. (Here, the perturber lies on the equatorial plane.)Thus we focus on a subset of points in our figure 4. Then for our calculations, we find that the minimal value, maximal value and mean value of the relative error, as described in equation (42), are given by 0.0000261744, 0.000612967 and 0.000275261 respectively. Indeed, using the mean value of the relative error as a comparison, we find a relative error of 0.002% where the previous paper found an error of 0.01%.[29].

For the case with a dynamic perturber, the results look very similar. As can be seen in figure 5, the results are less accurate compared to the stationary case with a minimal value, maximal value and mean value of the relative error of 0.000144949, 0.000551504 and 0.000347293 respectively. Comparing the mean averages, the dynamic case is still accurate within an error of 0.03% for the similar case as the 0.01% in [29].

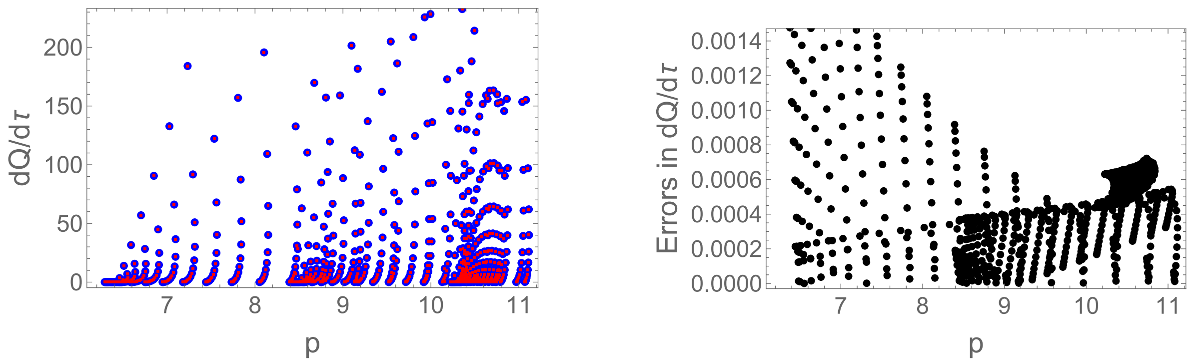

(a) ***(b)***

Figure 5: *Application of the two-for-one deal for jumps in the Carter constant Q induced by a* ***dynamic perturber*** *for the resonance number combination* $(3, 0, -2, 2)$. *The left plot compares the values for Q as calculated using the two-for-one deal relation (denoted by the red blocks) and as calculated using the jump size calculations (denoted by the blue circles). The vertical axis shows the jump sizes and the horizontal axis shows the value of p for which the resonance occurs. On the right we plot the relative error for each set, which is given by the absolute value of the relative difference between the two value of the left plot.*

It is however important to note that the right plots in this section show the **relative** error. This relative error will increase substantially when the value of Q becomes very small or goes to zero. This explains some of the higher relative errors for low values of p in figures 4 and 5. As we see in the left plot of figures 4 and 5, this jump goes to zero for small values of p, which is also when this relative error increases drastically. To better show this effect, figure 6 shows the same error as figure 4, but without dividing by the value of Q as in equation (42). Thus this shows the absolute error. Indeed, we see in this plot that these large errors, for small values of p, disappear.

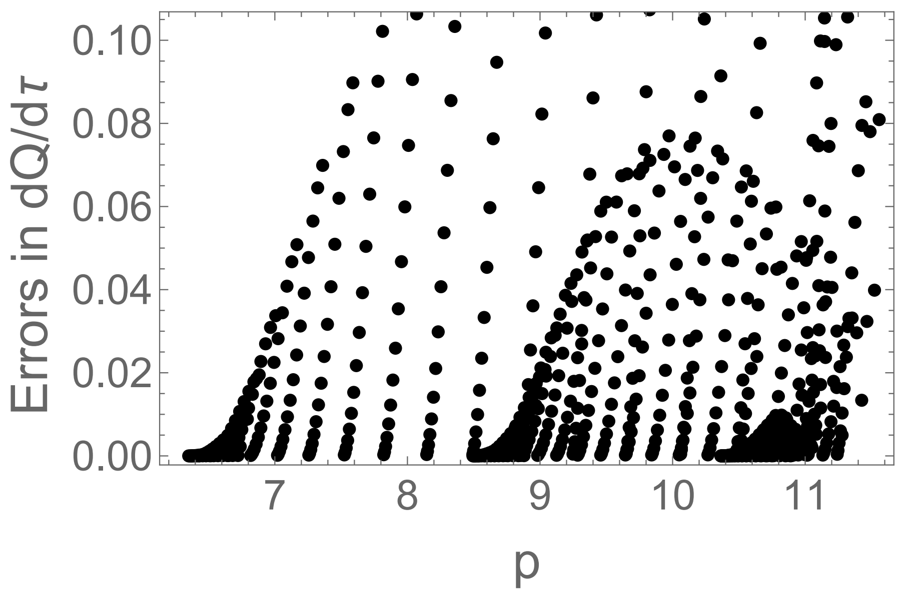

Figure 6: *The absolute error of the tidal jumps in the Carter constant Q induced by a* ***stationary perturber*** *for the resonance number combination (3,0,-2), which is given by the absolute value of the difference between the two differently calculated values of Q from figure 4.*

More results for a variety of resonance number combinations can be found in appendix A. These results vary a lot between different resonances and different values of a, e, x. For example, we can distinctly see that for the (1,2,-2) resonance in figure 11, there is a larger relative error then usual. This is noteworthy and shows that the two-for-one deal does not perform equally as good for all resonances. However, the trend still persists that the errors for a dynamic calculation are of similar order as those of the stationary case. Thus, these results show that this two-for-one deal is still quite accurate for the dynamic approach, despite the fact that it strictly does not apply in this scenario, and could be used in the future of tidal resonance research to greatly reduce computation time.

4 The effect of changing Ω_{td}

In this section, we will provide the theoretical background behind the other main interest of this thesis, the orbital frequency of the tidal perturber, Ω_{td}. Specifically, we are interested to see how the tidal jump changes when changing this Ω_{td}. In this section, we will introduce the equations that are crucial for investigating this effect. Then, we will show how the calculation of the jump sizes depends on Ω_{td} in various ways. Despite these various dependencies, we find that changing Ω_{td} gives much more predictable results than initially expected. Finally, we will present additional challenges that still persist when taking into account the effect of Ω_{td} in the tidal jump calculations.

4.1 Theory

First of all, Ω_{td} is defined as the orbital frequency of the tidal perturber. Thus, in terms of the mass of the central BH of the EMRI M, the mass of the perturber M_* and the distance between them b, it is defined as [19]

$$\Omega_{\text{td}} = \frac{GM}{c^3}\sqrt{\frac{G(M+M_*)}{b^3}} + 1\text{PN}, \tag{43}$$

where G is the gravitational constant and c is the speed of light. The factor $\frac{GM}{c^3}$ simply acts to make the frequency dimensionless. As can be seen, we are only interested in the zeroth order PN contributions. This is because the first order PN contribution already scales with the perturber's orbital velocity squared, which is small in our region of interest where $M \ll b$ [19].

Secondly, as we have already seen in equation (4), we can approximate the tidal jump using an adiabatic approximation. We write this now in terms of the orbital constants of motion $\mathcal{C}$, like we did in equation (27). Such that it is given by [11]

$$\frac{d\mathcal{C}}{d\tau} \approx \epsilon \left\langle G_i^{(i)}(q_r, q_\theta, q_\phi, \boldsymbol{\mathcal{C}}) \right\rangle, \tag{44}$$

where ϵ is the tidal field strength parameter in which the equations of motion were expanded in section 2.1, which was given by

$$\epsilon = \frac{G^3}{c^6}\frac{M_* M^2}{b^3}. \tag{45}$$

The perturber will be considered stationary as long as the resonance duration is much shorter than the orbital period of the perturber. The resonance duration τ_{res} and the orbital period

T_{td} of the perturber are given by [19]

$$\begin{aligned} \tau_{res} &= \sqrt{\tfrac{4\pi}{|\Gamma|}} \sim M\sqrt{\tfrac{1}{\eta}}, \\ T_{td} &= \tfrac{2\pi}{\Omega_{\mathrm{td}}}. \end{aligned} \tag{46}$$

Thus, the perturber is considered stationary as long as $\tau_{res} \ll T_{td}$.

4.2 Dependencies on Ω_{td} in the jump calculation

The orbital frequency of the tidal perturber, Ω_{td}, arises in multiple instances during the calculation of the tidal jumps.
Most importantly, Ω_{td} is an explicit part of the resonance condition for dynamic perturbers, as given by equation (7). Therefore, the value of Ω_{td} directly determines the orbital parameters (a, p, e, x) for which a particular (n, k, m, s) resonance will occur. In other words, a change in Ω_{td} shifts the location of the resonance, i.e. at which semi-latus rectum p the resonance condition is satisfied during the inspiral of the EMRI.
Beyond this, Ω_{td} also affects the calculation of the tidal jumps at other points during the calculation. First, because Ω_{td} changes p, this also changes the values for E, L_z and Q prior to the resonance.
Secondly, by changing p, we change the orbit $t(\lambda)$,$r(\lambda)$,$\theta(\lambda)$ and $\phi(\lambda)$ as we determined in chapter 2.3.2. Similarly, this changes the temporal and radial Mino-time frequencies from equation (24).
On top of this, Ω_{td} is a function of the mass of the central BH M, the mass of the tidal perturber M_* and the distance between them b. Similarly, the field strength parameter ϵ is also a function of these three parameters, according to equation (45). Thus, by varying Ω_{td}(, by changing one or more of these parameters), we also vary the field strength parameter ϵ. This also greatly influences the tidal jump calculation and thus changes the resulting jump in the orbital constants of motion.

4.3 Results

These various dependencies on Ω_{td} during the jump calculation suggest a complicated relation between them. Despite this, we observe a very predictable result. This can be explained through equation (44), which I will repeat here for clarity:

$$\frac{d\mathcal{C}_i}{d\tau} \approx \epsilon \left\langle G_i^{(i)}(q_r, q_\theta, q_\phi, \boldsymbol{J}) \right\rangle . \tag{47}$$

The dependencies as discussed in section 4.2, all arise in the second part of this equation in the orbital averaging of the tidal force. However, they all appear inside trigonometric functions. Consequently, when performing the orbital averaging, denoted by the angular brackets, these contributions are suppressed. We are left with the Ω_{td} inside ϵ that mainly contributes to the Ω_{td} dependency of the jump size $\frac{d\mathcal{C}_i}{d\tau}$.
In order to test this, we choose fixed values for the parameters a, p, e, x and focus on one resonance by choosing n, k, m, s. Then, we vary the values of M_* and b, which are two of the main components of Ω_{td}. (We kept M fixed, since this has a more complicated effect.) By looking at equations (43), (44) and (45), we expect a quadratic dependency on Ω_{td} for the tidal jumps, so $\frac{d\mathcal{C}_i}{d\tau} \sim \Omega_{\text{td}}^2$.

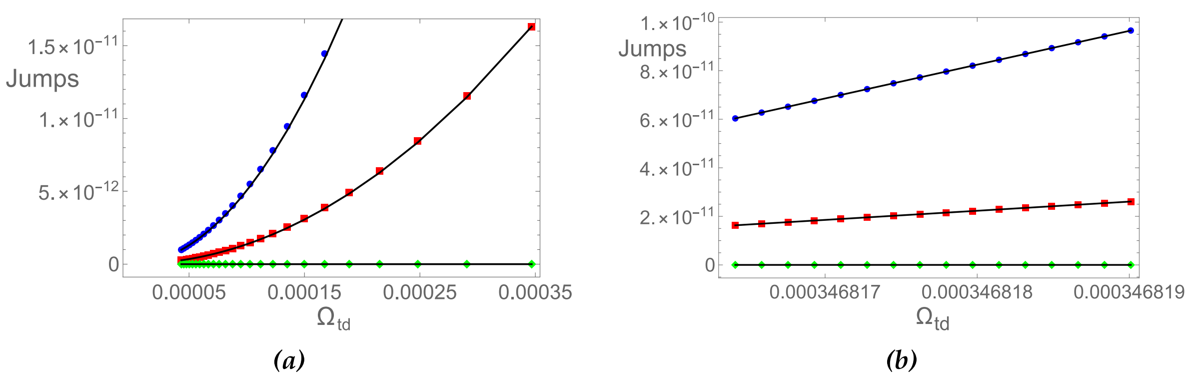

Figure 7: *Plot showing the jumps in E, L, Q in green, blue and red respectively. The jumps are calculated for the (3,0,-2,2) resonance with (a,e,x)=(0.5,0.5,0.5), while ranging 2 AU$\leq$ b $\leq$8 AU and 25 $\mathrm{M}_\odot \leq$ M_* $\leq$40 $\mathrm{M}_\odot$. The plot shows Ω_{td} on the horizontal axis and the jump sizes on the vertical axis. On the left, we vary Ω_{td} by changing only the distance b, on the right we vary Ω_{td} by changing only the mass M_*.*

As can be seen in figure 7, the results align with this quadratic dependency we expected. On the left side, we show how the jump changes when only varying b and keeping M_* fixed, while on the right side we vary M_* while keeping b fixed. These plots were calculated for the resonance with $(n, k, m, s) = (3, 0, -2, 2)$.

4.4 Additional Challenges

In the previous section, we showed that a predictable quadratic relationship can be found between the jump amplitudes and the values of Ω_{td}. However, other additional challenges that arise due to the influence of Ω_{td} still remain. This section will discuss them and show that more research is needed to obtain the full picture of the influence of Ω_{td}.

In the stationary case, when $s = 0$, a resonance occurs when $n\omega_r + k\omega_\theta + m\omega_\phi = 0$. For a given set of resonance numbers (n, k, m), we observe that this condition is only met at a single, unique value of the semi-latus rectum p, during the inspiral.
The situation becomes more complex in the dynamic case, where the resonance condition is $n\omega_r + k\omega_\theta + m\omega_\phi + s\Omega_{\text{td}} = 0$. The term $s\Omega_{\text{td}}$ is constant for a given perturber and acts as a vertical offset to the resonance condition function. This is shown in figure 8, which plots the value of the resonance condition as a function of p, first increasing before slowly decreasing and converging to a constant value. On the left, we see the resonance condition for the stationary case with $(n, k, m, a, e, x) = (3, -4, 2, 0.78, 0.85, 0.78)$, while on the right side, we see the corresponding dynamic case with $s = -2$. In the stationary case, we observe that this curve only converges to a positive value after this maximum. Meaning that the curve only crosses the horizontal axis once. However, by introducing a non-zero $s\Omega_{\text{td}}$, we effectively shift this entire curve up (for $s\Omega_{\text{td}} > 0$) or down (for $s\Omega_{\text{td}} < 0$). This can cause the curve to intersect the horizontal axis at two distinct points. This implies that an inspiraling object can pass through the same (n, k, m, s) resonance twice during its evolution, once at an early semi-latus rectum p_1 and again at a later p_2. This possibility of multiple encounters with the same resonance type complicates the evolution of the inspiral.

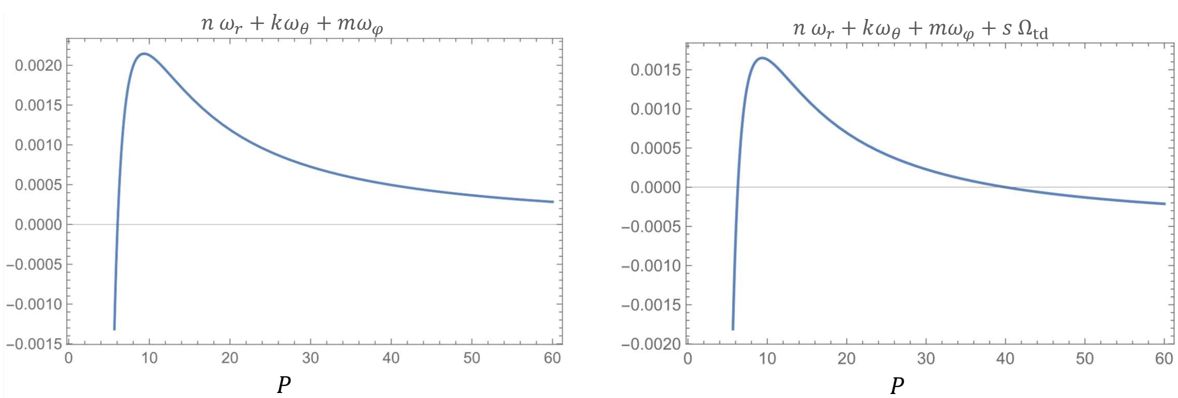

(a) ***(b)***

Figure 8: *A plot showing the resonance condition as a function of p. Any zero-crossing of the line indicates the resonance condition is satisfied and a tidal resonance occurs. On the left, we see (n,k,m,a,e,x)=(3,-4,2,0.78,0.85,0.78) and on the right we see that corresponding dynamic case with s=-2 and* $\Omega_{td} = 0.000248159$.

Furthermore, there are two particularly noteworthy trends in figure 8. Firstly, the graph seems to converge at large values of p. This is because, for large values of p, the system enters the weak-field regime where the different orbital frequencies, ω_r, ω_θ and ω_ϕ become degenerate and coincide with the Keplerian frequency ω_K [14]. Thus this graph converges to the sum of the integer resonance numbers times this Keplerian frequency. Secondly, it is interesting to note that for low values of p, the graph tends to decrease greatly. This is because below the separatrix the theory breaks down. This is where the frequencies strongly deviate from each other and the bound orbit turns into a plunge orbit. Specifically, the graph goes to minus infinity. This can be explained by the fact that the value of ω_r tends to negative infinity for low values of p, whereas the values of ω_θ and ω_ϕ go to positive infinity, as seen in figure 7 from [17]. Since n is the most dominant resonance number in this system, the trend from ω_r dominates and the graph tends to negative infinity.

Finally, this shifting mechanism also reveals another key observation; that some dynamic resonances do not have a stationary counterpart. It is possible for the stationary resonance function, where $s = 0$, to lie entirely above or below the horizontal axis (for all values of p above the separatrix). However, a sufficiently large $s\Omega_{\text{td}}$ term can shift the curve to create a zero-crossing, thus enabling a dynamic resonance without corresponding stationary resonance. This demonstrates that the dynamic case does not merely perturb the locations of the corresponding stationary resonances, but can also introduce new resonances that are absent in the stationary case. These phenomena will be crucial during future tidal resonance research. Accurately modeling EMRI waveforms will require identifying all possible resonance locations, including the potential for multiple crossings for a single resonance number combination and those resonances unique to the dynamic case but absent in the stationary case.

5 Discussion and Outlook

This thesis utilized a theoretical framework to study tidal resonances in EMRIs, with a specific focus on the dynamic case. Our investigation resulted in two key results. First, we validated the "two-for-one deal" for dynamic perturbers, confirming that this relation accurately connects the jumps in the Carter constant Q and the angular momentum L_z. This result offers a significant computational simplification for future studies. Despite this, we remain uncertain on the impact of an uncertainty of this size on the uncertainty in the corresponding waveforms. Implementation of these effects on the waveform construction will show whether this effect is indeed small enough to be neglected or, whether it will still show its effects in the resulting waveform.

Second, we analyzed the influence of the perturber's orbital frequency, Ω_{td}, on the jump amplitudes, finding a predictable quadratic relationship when changing Ω_{td} by altering b or M_*. This predictable relationship will help reduce computational cost of further efforts in tidal resonance research. On top of this, we discussed additional challenges in section 4.4. Namely, in the dynamic case the orbital frequency Ω_{td} can shift the resonance condition, leading to two main challenges. An inspiraling object may pass through the same resonance twice and some dynamic resonances can be excited even when no corresponding stationary resonance exists. These complexities still arise due to the effect of Ω_{td} and have to be taken into account.

Furthermore, a crucial part of our discussion is the definition of Ω_{td}. That is, we defined this as $\Omega_{\text{td}} = \frac{dQ_{\text{td}}}{dt}$ in section 2.2. However, in order to correctly compare the frequency with the fundamental frequencies of the EMRI's secondary mass, we must define it in terms of proper time τ [17], such that

$$\tilde{\Omega}_{\text{td}} = \frac{dQ_{\text{td}}}{d\tau} = \Omega_{\text{td}} \frac{dt}{d\tau}. \tag{48}$$

Thus, this adds a factor $\frac{dt}{d\tau}$, which will change the tidal jump calculations that were done for the case with a dynamic perturber. However, the only change induced by this factor is when along the inspiral the resonance happens, i.e. for which value of the semi latus rectum p. It does not change the amplitudes of the tidal jumps. This is because the calculation of the acceleration in section 2.3.1 is dependent on Ω_{td} and not $\tilde{\Omega}_{\text{td}}$. On top of this, the value of the field strength parameter ϵ will not change because of this, thus we expect our analysis from chapter 4 to remain intact after this is considered. Nonetheless, it could still substantially influence other parts of the research within this thesis, such as the two-for-one deal analysis and the additional challenges induced by Ω_{td}.

Once this is taken into account, the next step for this research will be to implement the calculated tidal jumps into the Fast EMRI Waveform (FEW) python package, a key component of the Black Hole Perturbation Toolkit (BHPT). Current waveform models typically describe isolated EMRIs, neglecting environmental effects like tidal perturbations. By implementing these jumps, we can construct more physically accurate waveforms for LISA. This implementation will allow us to answer crucial questions: What is the cumulative effect of tidal resonances on the gravitational waves? Can we use these signatures to distinguish between an isolated EMRI and one in a populated galactic nucleus? This could enable LISA to not only detect EMRIs but also to probe the environments of supermassive BHs.

To complete the implementation, further research should also systematically map the resonance locations discussed in section 4.4. This means cataloging all possible resonance crossings, including multiple encounters and dynamic-only resonances, for a given inspiral.

Together, these efforts will help developing the waveform models necessary to accurately interpret the future data from LISA.

References

[1] The LIGO Scientific Collaboration and the Virgo Collaboration. Observation of Gravitational Waves from a Binary Black Hole Merger. 116(6):061102.

[2] Monica Colpi, Danzmann Karsten, and et al. Lisa definition study report, 2024.

[3] Pau Amaro-Seoane, Heather Audley, and et al. Laser Interferometer Space Antenna.

[4] Piotr Jaranowski and Andrzej Królak. Gravitational-Wave Data Analysis. Formalism and Sample Applications: The Gaussian Case. 15(1):4.

[5] Michele Maggiore. *Gravitational Waves: Volume 2: Astrophysics and Cosmology*. Oxford University PressOxford, March 2018.

[6] Philip Lynch and Maarten van de Meent. Self-forced inspirals with spin-orbit precession. 109(8):084072.

[7] Smadar Naoz and Zoltan Haiman. The Enhanced Population of Extreme Mass-Ratio Inspirals in the LISA Band from Supermassive Black Hole Binaries.

[8] Black Hole Perturbation Toolkit. (bhptoolkit.org).

[9] Morteza Kerachian, Lukáš Polcar, Viktor Skoupý, Christos Efthymiopoulos, and Georgios Lukes-Gerakopoulos. Action-angle formalism for extreme mass ratio inspirals in kerr spacetime. 108(4):044004.

[10] Priti Gupta, Béatrice Bonga, Alvin J. K. Chua, and Takahiro Tanaka. Importance of tidal resonances in extreme-mass-ratio inspirals. 104(4):044056.

[11] Priti Gupta, Lorenzo Speri, Béatrice Bonga, Alvin J. K. Chua, and Takahiro Tanaka. Modeling transient resonances in extreme-mass-ratio inspirals. 106(10):104001.

[12] Tanja Hinderer and Éanna É. Flanagan. Two-timescale analysis of extreme mass ratio inspirals in Kerr spacetime: Orbital motion. 78(6):064028.

[13] Scott A. Hughes, Steve Drasco, Éanna É. Flanagan, and Joel Franklin. Gravitational Radiation Reaction and Inspiral Waveforms in the Adiabatic Limit. 94(22):221101.

[14] W. Schmidt. Celestial mechanics in Kerr spacetime. 19.

[15] Béatrice Bonga, Huan Yang, and Scott A. Hughes. Tidal resonance in extreme mass-ratio inspirals. *Physical Review*, 123(10):101103, 2019.

[16] Priti Gupta, Lorenzo Speri, Béatrice Bonga, Alvin J. K. Chua, and Takahiro Tanaka. Modeling transient resonances in extreme-mass-ratio inspirals. 106(10):104001.

[17] Bart Peters. Tidal resonances in extreme mass ratio inspirals. Master's thesis, Radboud University, Nijmegen, The Netherlands, July 2023. Available at `https://hef.ru.nl/~bbonga/documents/Thesis-Bart_Peters.pdf`.

[18] Eric Poisson and Igor Vlasov. Geometry and dynamics of a tidally deformed black hole. 81(2):024029.

[19] Stephanne Taylor and Eric Poisson. Nonrotating black hole in a post-Newtonian tidal environment. 78(8):084016.

[20] Clifford M. Will. Gravity: Newtonian, Post-Newtonian, and General Relativistic. In Roberto Peron, Monica Colpi, Vittorio Gorini, and Ugo Moschella, editors, *Gravity: Where Do We Stand?*, pages 9–72.

[21] Philippe Landry and Eric Poisson. Tidal deformation of a slowly rotating material body. External metric. 91(10):104018.

[22] Zachary Nasipak. Adiabatic evolution due to the conservative scalar self-force during orbital resonances. 106(6):064042.

[23] Steve Drasco, Eanna E. Flanagan, and Scott A. Hughes. Computing inspirals in Kerr in the adiabatic regime. I. The scalar case. 22(15):S801–S846.

[24] Yasushi Mino. Perturbative approach to an orbital evolution around a supermassive black hole. 67(8):084027.

[25] Ryuichi Fujita and Wataru Hikida. Analytical solutions of bound timelike geodesic orbits in kerr spacetime. 26(13):135002.

[26] Éanna É. Flanagan and Tanja Hinderer. Transient Resonances in the Inspirals of Point Particles into Black Holes. 109(7):071102.

[27] Makana Silva and Christopher Hirata. Dynamical perturbations around an extreme mass ratio inspiral near resonance. 106(8):084058.

[28] Lorenzo Speri and Jonathan R. Gair. Assessing the impact of transient orbital resonances. 103(12):124032.

[29] Priti Gupta, Takafumi Kakehi, and Takahiro Tanaka. Resonant jumps induced by stationary tidal perturbation: a two-for-one deal. 39(24):245005.

[30] Herbert Goldstein, Charles P. Poole, Jr., and John L. Safko. *Classical Mechanics*. Addison Wesley, San Francisco, CA, 3rd edition, 2002.

A Appendix: Extra results two-for-one deal

In appendix A, we will show extra plots of the two-for-one deal results from chapter 3. These results are given to further support chapter 3 by showing its accuracy for different resonance number combinations. Figure 9 shows results for a stationary resonance with $(n, k, m) = (3, -4, 2)$ and figure 10 shows that for a dynamic resonance with $(n, k, m, s) = (3, -4, 2, 2)$. Figures 11 and 12 show the same for$(n, k, m) = (1, 2, -2)$ and $(n, k, m) = (1, 2, -2, 2)$ and 13 and 14 show the same for$(n, k, m) = (4, -1, -1)$ and $(n, k, m) = (4, -1, -1, 2)$.

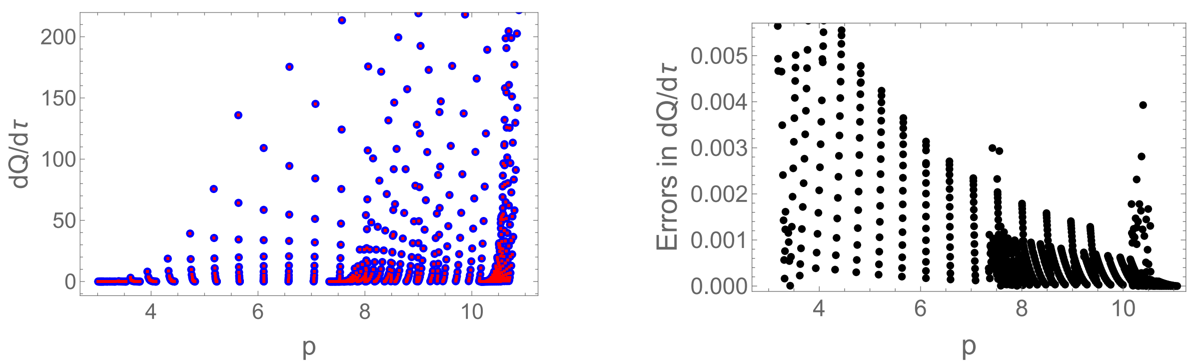

(a) *(b)*

Figure 9: *Validation of the two-for-one deal for jumps in the Carter constant Q induced by a* ***stationary perturber*** *for the resonance number combination $(3, -4, 2)$. The left plot compares the values for Q as calculated using the two-for-one deal relation (denoted by the red blocks) and as calculated using the jump size calculations (denoted by the blue circles). The vertical axis shows the jump sizes and the horizontal axis shows the value of p for which the resonance occurs. On the right we plot the relative error for each set, which is given by the absolute value of the relative difference between the two value of the left plot.*

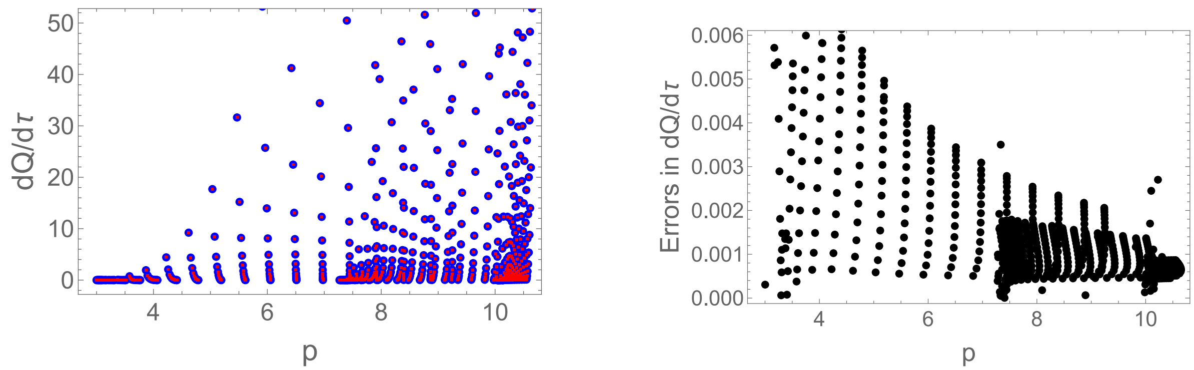

(a) ***(b)***

Figure 10: *Application of the two-for-one deal for jumps in the Carter constant Q induced by a* ***dynamic perturber*** *for the resonance number combination* $(3, -4, 2, 2)$*. The left plot compares the values for Q as calculated using the two-for-one deal relation (denoted by the red blocks) and as calculated using the jump size calculations (denoted by the blue circles). The vertical axis shows the jump sizes and the horizontal axis shows the value of p for which the resonance occurs. On the right we plot the relative error for each set, which is given by the absolute value of the relative difference between the two value of the left plot.*

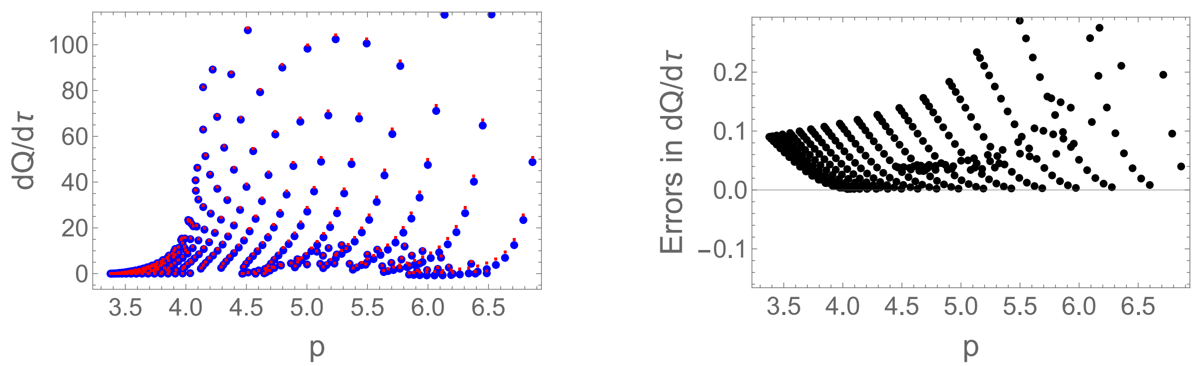

(a) ***(b)***

Figure 11: *Validation of the two-for-one deal for jumps in the Carter constant Q induced by a* ***stationary perturber*** *for the resonance number combination* $(1, 2, -2)$*. The left plot compares the values for Q as calculated using the two-for-one deal relation (denoted by the red blocks) and as calculated using the jump size calculations (denoted by the blue circles). The vertical axis shows the jump sizes and the horizontal axis shows the value of p for which the resonance occurs. On the right we plot the relative error for each set, which is given by the absolute value of the relative difference between the two value of the left plot.*

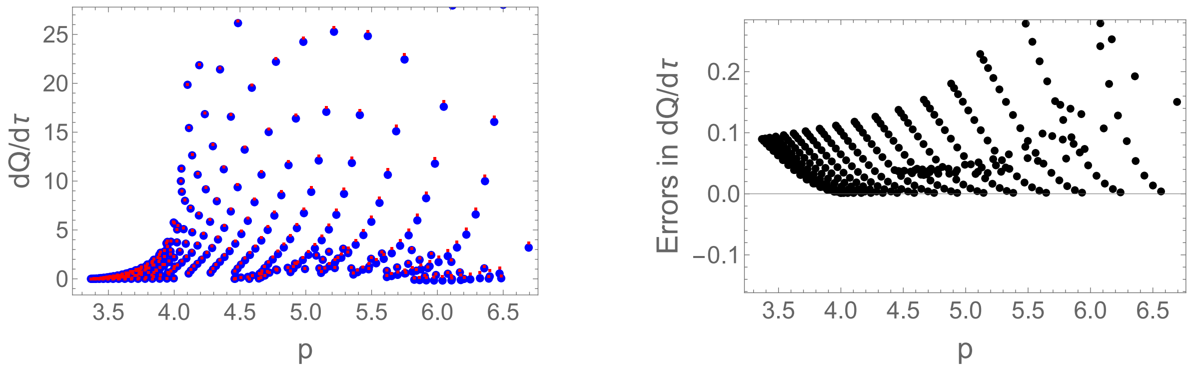

(a) ***(b)***

Figure 12: *Application of the two-for-one deal for jumps in the Carter constant Q induced by a* ***dynamic perturber*** *for the resonance number combination* $(1, 2, -2, 2)$. *The left plot compares the values for Q as calculated using the two-for-one deal relation (denoted by the red blocks) and as calculated using the jump size calculations (denoted by the blue circles). The vertical axis shows the jump sizes and the horizontal axis shows the value of p for which the resonance occurs. On the right we plot the relative error for each set, which is given by the absolute value of the relative difference between the two value of the left plot.*

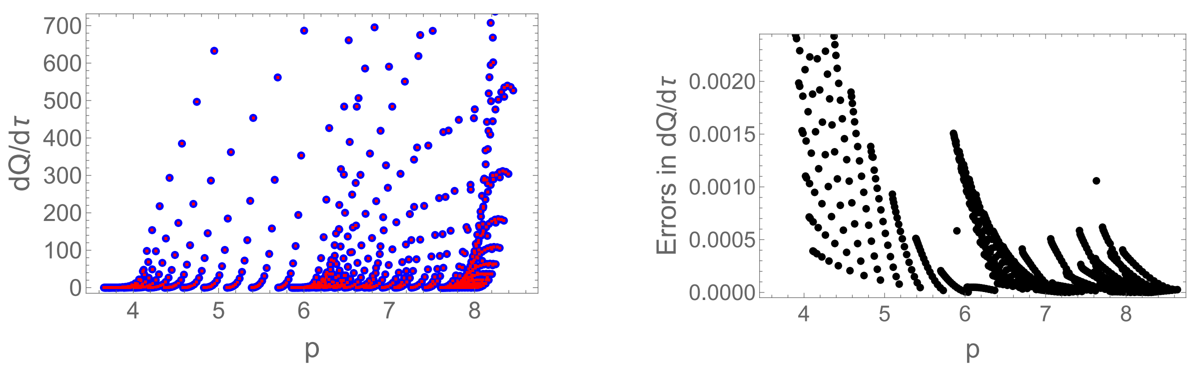

(a) ***(b)***

Figure 13: *Validation of the two-for-one deal for jumps in the Carter constant Q induced by a* ***stationary perturber*** *for the resonance number combination* $(4, -1, -1)$. *The left plot compares the values for Q as calculated using the two-for-one deal relation (denoted by the red blocks) and as calculated using the jump size calculations (denoted by the blue circles). The vertical axis shows the jump sizes and the horizontal axis shows the value of p for which the resonance occurs. On the right we plot the relative error for each set, which is given by the absolute value of the relative difference between the two value of the left plot.*

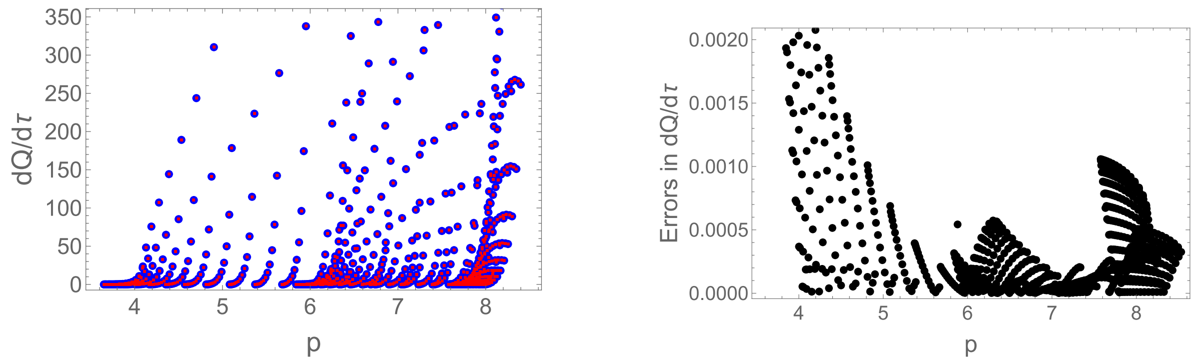

(a) *(b)*

Figure 14: *Application of the two-for-one deal for jumps in the Carter constant Q induced by a* ***dynamic perturber*** *for the resonance number combination* $(4, -1, -1, 2)$. *The left plot compares the values for Q as calculated using the two-for-one deal relation (denoted by the red blocks) and as calculated using the jump size calculations (denoted by the blue circles). The vertical axis shows the jump sizes and the horizontal axis shows the value of p for which the resonance occurs. On the right we plot the relative error for each set, which is given by the absolute value of the relative difference between the two value of the left plot.*

Finally, we show similar results for two dynamic resonances that do not have a stationary counterpart, namely (2,1,-2,1) and (3,1,-2,1). As seen in figures 15 and 16, these do perform worse then the other plots in this Appendix.

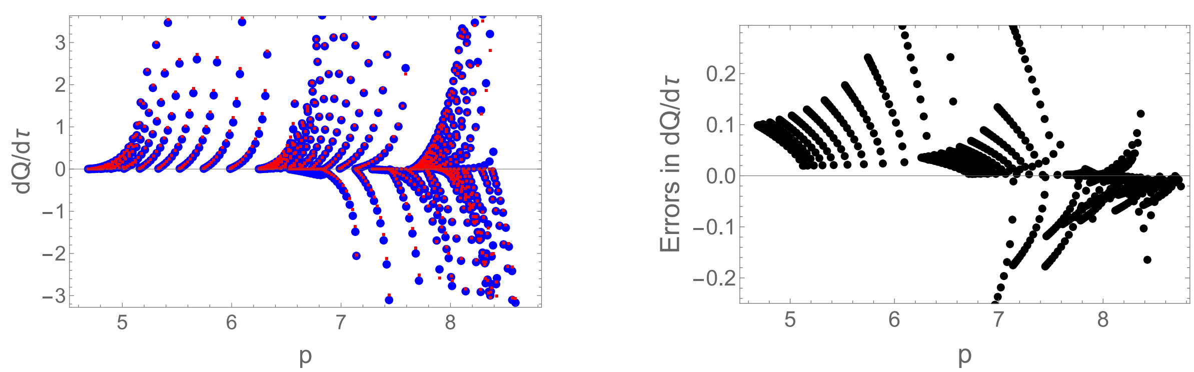

(a) *(b)*

Figure 15: *Application of the two-for-one deal for jumps in the Carter constant Q induced by a* ***dynamic perturber*** *for the resonance number combination* $(2, 1, -2, 1)$. *The left plot compares the values for Q as calculated using the two-for-one deal relation (denoted by the red blocks) and as calculated using the jump size calculations (denoted by the blue circles). The vertical axis shows the jump sizes and the horizontal axis shows the value of p for which the resonance occurs. On the right we plot the relative error for each set, which is given by the absolute value of the relative difference between the two value of the left plot.*

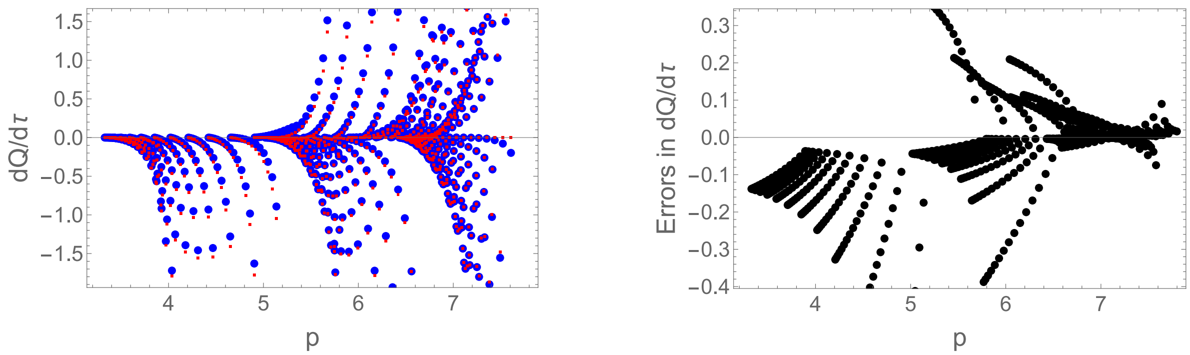

(a)

(b)

Figure 16: *Application of the two-for-one deal for jumps in the Carter constant Q induced by a* ***dynamic perturber*** *for the resonance number combination $(3, 1, -2, 1)$. The left plot compares the values for Q as calculated using the two-for-one deal relation (denoted by the red blocks) and as calculated using the jump size calculations (denoted by the blue circles). The vertical axis shows the jump sizes and the horizontal axis shows the value of p for which the resonance occurs. On the right we plot the relative error for each set, which is given by the absolute value of the relative difference between the two value of the left plot.*

In table 1 we provide all the total mean relative errors and mean relative errors for the particular case when we set $e = 0.7$ and $x = 0.96$, for all the examined resonance number combinations. In this table, the rows with resonance numbers where only (n, k, m) are specified, are the stationary case resonances.

(n,k,m,s)	Total Mean Relative Error	Mean Relative Error (e=0.7, x=0.96)
(3,0,-2)	0.00049677	0.000275261
(3,0,-2,2)	0.000506583	0.000347293
(3,-4,2)	0.0190623	0.00284616
(3,-4,2,2)	0.00508755	0.00055887
(1,2,-2)	0.124472	0.0118447
(1,2,-2,2)	0.119161	0.0112888
(4,-1,-1)	0.000576968	0.000558002
(4,-1,-1,2)	0.000512527	0.000618386
(2,1,-2,1)	15.3986	0.0234015
(3,1,-2,1)	-9.51319	-0.0317263

Table 1: *A table showing all total mean relative errors and mean relative errors for the particular case when we set $e = 0.7$ and $x = 0.96$, for all the examined resonance number combinations.*

B Appendix: Relevant resonance number combinations

In this section we provide the selection process and Mathematica code used to filter the relevant resonance number combinations (n, k, m, s) that will satisfy the resonance condition from equation (7). This selection process involves several filtering steps to apply physical and mathematical constraints. An important separation we make in this section is the one between the case with a perturber in prograde motion or retrograde motion. We will start by looking at the stationary case, since this is the least complex. In prograde motion, the selection rules looks like:

- We cannot have only positive integers for (n, k, m)
- The general selection rule: $k + m = \text{even}$
- Take n to be positive because everything times - 1 gives the same resonance
- if $n = 0$, take k to be positive because everything times -1 gives the same resonance

The number of (n, k, m) combinations for the stationary case in prograde motion is 44, and they are given by:

$$
\begin{array}{lllll}
(0,1,-1), & (0,3,-1), & (1,-4,-2), & (1,-4,0), & (1,-4,2), \\
(1,-3,-1), & (1,-3,1), & (1,-2,-2), & (1,-2,0), & (1,-2,2), \\
(1,-1,-1), & (1,-1,1), & (1,0,-2), & (1,1,-1), & (1,2,-2), \\
(1,3,-1), & (1,4,-2), & (2,-3,-1), & (2,-3,1), & (2,-1,-1), \\
(2,-1,1), & (2,1,-1), & (2,3,-1), & (3,-4,-2), & (3,-4,0), \\
(3,-4,2), & (3,-3,-1), & (3,-3,1), & (3,-2,-2), & (3,-2,0), \\
(3,-2,2), & (3,-1,-1), & (3,-1,1), & (3,0,-2), & (3,1,-1), \\
(3,2,-2), & (3,3,-1), & (3,4,-2), & (4,-3,-1), & (4,-3,1), \\
(4,-1,-1), & (4,-1,1), & (4,1,-1), & (4,3,-1). &
\end{array}
$$

In retrograde motion, the selection looks like:

- We cannot have positive integers for n and k and negative for m, because $\omega_\phi < 0$
- The general selection rule: $k + m = \text{even}$
- Take n to be positive because everything times - 1 gives the same resonance
- if $n = 0$, take k to be positive because everything times -1 gives the same resonance

The number of (n, k, m) combinations for the stationary case in retrograde motion is also 44, and they are given by:

$(0,1,1)$,	$(0,3,1)$,	$(1,-4,-2)$,	$(1,-4,0)$,	$(1,-4,2)$,
$(1,-3,-1)$,	$(1,-3,1)$,	$(1,-2,-2)$,	$(1,-2,0)$,	$(1,-2,2)$,
$(1,-1,-1)$,	$(1,-1,1)$,	$(1,0,2)$,	$(1,1,1)$,	$(1,2,2)$,
$(1,3,1)$,	$(1,4,2)$,	$(2,-3,-1)$,	$(2,-3,1)$,	$(2,-1,-1)$,
$(2,-1,1)$,	$(2,1,1)$,	$(2,3,1)$,	$(3,-4,-2)$,	$(3,-4,0)$,
$(3,-4,2)$,	$(3,-3,-1)$,	$(3,-3,1)$,	$(3,-2,-2)$,	$(3,-2,0)$,
$(3,-2,2)$,	$(3,-1,-1)$,	$(3,-1,1)$,	$(3,0,2)$,	$(3,1,1)$,
$(3,2,2)$,	$(3,3,1)$,	$(3,4,2)$,	$(4,-3,-1)$,	$(4,-3,1)$,
$(4,-1,-1)$,	$(4,-1,1)$,	$(4,1,1)$,	$(4,3,1)$.	

Now we focus on the more complex dynamic case, starting by looking at the case with prograde motion. This follows the following selection rules:

- We cannot have only positive integers for (n, k, m, s)
- The general selection rule: $k + m + s = \text{even}$
- Take n to be positive because everything times - 1 gives the same resonance
- if $n = 0$, take k to be positive because everything times -1 gives the same resonance
- if $n = 0$ and $k = 0$, take m to be positive because everything times -1 gives the same resonance
- if $n = 0$, $k = 0$ and $m = 0$, take s to be positive because everything times -1 gives the same resonance
- multiple of one n, k, m, s combination do not contribute, we only consider the lowest order

The number of (n, k, m) combinations for the dynamic case in prograde motion is 354, and they are given by:

$(0,0,1,-1)$,	$(0,1,-2,-1)$,	$(0,1,-2,1)$,	$(0,1,-1,-2)$,	$(0,1,-1,0)$,	$(0,1,-1,2)$,
$(0,1,0,-1)$,	$(0,1,1,-2)$,	$(0,1,2,-1)$,	$(0,2,-2,-2)$,	$(0,2,-2,2)$,	$(0,2,-1,-1)$,
$(0,2,-1,1)$,	$(0,2,1,-1)$,	$(0,2,2,-2)$,	$(0,3,-2,-1)$,	$(0,3,-2,1)$,	$(0,3,-1,-2)$,
$(0,3,-1,0)$,	$(0,3,-1,2)$,	$(0,3,0,-1)$,	$(0,3,1,-2)$,	$(0,3,2,-1)$,	$(0,4,-2,0)$,
$(0,4,-1,-1)$,	$(0,4,-1,1)$,	$(0,4,0,-2)$,	$(0,4,1,-1)$,	$(1,-4,-2,-2)$,	$(1,-4,-2,0)$,
$(1,-4,-2,2)$,	$(1,-4,-1,-1)$,	$(1,-4,-1,1)$,	$(1,-4,0,-2)$,	$(1,-4,0,0)$,	$(1,-4,0,2)$,
$(1,-4,1,-1)$,	$(1,-4,1,1)$,	$(1,-4,2,-2)$,	$(1,-4,2,0)$,	$(1,-4,2,2)$,	$(1,-3,-2,-1)$,

$(1,-3,-2,1)$,	$(1,-3,-1,-2)$,	$(1,-3,-1,0)$,	$(1,-3,-1,2)$,	$(1,-3,0,-1)$,	$(1,-3,0,1)$,
$(1,-3,1,-2)$,	$(1,-3,1,0)$,	$(1,-3,1,2)$,	$(1,-3,2,-1)$,	$(1,-3,2,1)$,	$(1,-2,-2,-2)$,
$(1,-2,-2,0)$,	$(1,-2,-2,2)$,	$(1,-2,-1,-1)$,	$(1,-2,-1,1)$,	$(1,-2,0,-2)$,	$(1,-2,0,0)$,
$(1,-2,0,2)$,	$(1,-2,1,-1)$,	$(1,-2,1,1)$,	$(1,-2,2,-2)$,	$(1,-2,2,0)$,	$(1,-2,2,2)$,
$(1,-1,-2,-1)$,	$(1,-1,-2,1)$,	$(1,-1,-1,-2)$,	$(1,-1,-1,0)$,	$(1,-1,-1,2)$,	$(1,-1,0,-1)$,
$(1,-1,0,1)$,	$(1,-1,1,-2)$,	$(1,-1,1,0)$,	$(1,-1,1,2)$,	$(1,-1,2,-1)$,	$(1,-1,2,1)$,
$(1,0,-2,-2)$,	$(1,0,-2,0)$,	$(1,0,-2,2)$,	$(1,0,-1,-1)$,	$(1,0,-1,1)$,	$(1,0,0,-2)$,
$(1,0,1,-1)$,	$(1,0,2,-2)$,	$(1,1,-2,-1)$,	$(1,1,-2,1)$,	$(1,1,-1,-2)$,	$(1,1,-1,0)$,
$(1,1,-1,2)$,	$(1,1,0,-1)$,	$(1,1,1,-2)$,	$(1,1,2,-1)$,	$(1,2,-2,-2)$,	$(1,2,-2,0)$,
$(1,2,-2,2)$,	$(1,2,-1,-1)$,	$(1,2,-1,1)$,	$(1,2,0,-2)$,	$(1,2,1,-1)$,	$(1,2,2,-2)$,
$(1,3,-2,-1)$,	$(1,3,-2,1)$,	$(1,3,-1,-2)$,	$(1,3,-1,0)$,	$(1,3,-1,2)$,	$(1,3,0,-1)$,
$(1,3,1,-2)$,	$(1,3,2,-1)$,	$(1,4,-2,-2)$,	$(1,4,-2,0)$,	$(1,4,-2,2)$,	$(1,4,-1,-1)$,
$(1,4,-1,1)$,	$(1,4,0,-2)$,	$(1,4,1,-1)$,	$(1,4,2,-2)$,	$(2,-4,-2,0)$,	$(2,-4,-1,-1)$,
$(2,-4,-1,1)$,	$(2,-4,0,-2)$,	$(2,-4,0,2)$,	$(2,-4,1,-1)$,	$(2,-4,1,1)$,	$(2,-4,2,0)$,
$(2,-3,-2,-1)$,	$(2,-3,-2,1)$,	$(2,-3,-1,-2)$,	$(2,-3,-1,0)$,	$(2,-3,-1,2)$,	$(2,-3,0,-1)$,
$(2,-3,0,1)$,	$(2,-3,1,-2)$,	$(2,-3,1,0)$,	$(2,-3,1,2)$,	$(2,-3,2,-1)$,	$(2,-3,2,1)$,
$(2,-2,-2,-2)$,	$(2,-2,-2,2)$,	$(2,-2,-1,-1)$,	$(2,-2,-1,1)$,	$(2,-2,0,0)$,	$(2,-2,1,-1)$,
$(2,-2,1,1)$,	$(2,-2,2,-2)$,	$(2,-2,2,2)$,	$(2,-1,-2,-1)$,	$(2,-1,-2,1)$,	$(2,-1,-1,-2)$,
$(2,-1,-1,0)$,	$(2,-1,-1,2)$,	$(2,-1,0,-1)$,	$(2,-1,0,1)$,	$(2,-1,1,-2)$,	$(2,-1,1,0)$,
$(2,-1,1,2)$,	$(2,-1,2,-1)$,	$(2,-1,2,1)$,	$(2,0,-2,0)$,	$(2,0,-1,-1)$,	$(2,0,-1,1)$,
$(2,0,0,-2)$,	$(2,0,1,-1)$,	$(2,1,-2,-1)$,	$(2,1,-2,1)$,	$(2,1,-1,-2)$,	$(2,1,-1,0)$,
$(2,1,-1,2)$,	$(2,1,0,-1)$,	$(2,1,1,-2)$,	$(2,1,2,-1)$,	$(2,2,-2,-2)$,	$(2,2,-2,2)$,
$(2,2,-1,-1)$,	$(2,2,-1,1)$,	$(2,2,1,-1)$,	$(2,2,2,-2)$,	$(2,3,-2,-1)$,	$(2,3,-2,1)$,
$(2,3,-1,-2)$,	$(2,3,-1,0)$,	$(2,3,-1,2)$,	$(2,3,0,-1)$,	$(2,3,1,-2)$,	$(2,3,2,-1)$,
$(2,4,-2,0)$,	$(2,4,-1,-1)$,	$(2,4,-1,1)$,	$(2,4,0,-2)$,	$(2,4,1,-1)$,	$(3,-4,-2,-2)$,
$(3,-4,-2,0)$,	$(3,-4,-2,2)$,	$(3,-4,-1,-1)$,	$(3,-4,-1,1)$,	$(3,-4,0,-2)$,	$(3,-4,0,0)$,
$(3,-4,0,2)$,	$(3,-4,1,-1)$,	$(3,-4,1,1)$,	$(3,-4,2,-2)$,	$(3,-4,2,0)$,	$(3,-4,2,2)$,
$(3,-3,-2,-1)$,	$(3,-3,-2,1)$,	$(3,-3,-1,-2)$,	$(3,-3,-1,0)$,	$(3,-3,-1,2)$,	$(3,-3,0,-1)$,
$(3,-3,0,1)$,	$(3,-3,1,-2)$,	$(3,-3,1,0)$,	$(3,-3,1,2)$,	$(3,-3,2,-1)$,	$(3,-3,2,1)$,
$(3,-2,-2,-2)$,	$(3,-2,-2,0)$,	$(3,-2,-2,2)$,	$(3,-2,-1,-1)$,	$(3,-2,-1,1)$,	$(3,-2,0,-2)$,
$(3,-2,0,0)$,	$(3,-2,0,2)$,	$(3,-2,1,-1)$,	$(3,-2,1,1)$,	$(3,-2,2,-2)$,	$(3,-2,2,0)$,
$(3,-2,2,2)$,	$(3,-1,-2,-1)$,	$(3,-1,-2,1)$,	$(3,-1,-1,-2)$,	$(3,-1,-1,0)$,	$(3,-1,-1,2)$,
$(3,-1,0,-1)$,	$(3,-1,0,1)$,	$(3,-1,1,-2)$,	$(3,-1,1,0)$,	$(3,-1,1,2)$,	$(3,-1,2,-1)$,
$(3,-1,2,1)$,	$(3,0,-2,-2)$,	$(3,0,-2,0)$,	$(3,0,-2,2)$,	$(3,0,-1,-1)$,	$(3,0,-1,1)$,
$(3,0,0,-2)$,	$(3,0,1,-1)$,	$(3,0,2,-2)$,	$(3,1,-2,-1)$,	$(3,1,-2,1)$,	$(3,1,-1,-2)$,
$(3,1,-1,0)$,	$(3,1,-1,2)$,	$(3,1,0,-1)$,	$(3,1,1,-2)$,	$(3,1,2,-1)$,	$(3,2,-2,-2)$,
$(3,2,-2,0)$,	$(3,2,-2,2)$,	$(3,2,-1,-1)$,	$(3,2,-1,1)$,	$(3,2,0,-2)$,	$(3,2,1,-1)$,
$(3,2,2,-2)$,	$(3,3,-2,-1)$,	$(3,3,-2,1)$,	$(3,3,-1,-2)$,	$(3,3,-1,0)$,	$(3,3,-1,2)$,
$(3,3,0,-1)$,	$(3,3,1,-2)$,	$(3,3,2,-1)$,	$(3,4,-2,-2)$,	$(3,4,-2,0)$,	$(3,4,-2,2)$,
$(3,4,-1,-1)$,	$(3,4,-1,1)$,	$(3,4,0,-2)$,	$(3,4,1,-1)$,	$(3,4,2,-2)$,	$(4,-4,-2,0)$,
$(4,-4,-1,-1)$,	$(4,-4,-1,1)$,	$(4,-4,0,-2)$,	$(4,-4,0,2)$,	$(4,-4,1,-1)$,	$(4,-4,1,1)$,
$(4,-4,2,0)$,	$(4,-3,-2,-1)$,	$(4,-3,-2,1)$,	$(4,-3,-1,-2)$,	$(4,-3,-1,0)$,	$(4,-3,-1,2)$,
$(4,-3,0,-1)$,	$(4,-3,0,1)$,	$(4,-3,1,-2)$,	$(4,-3,1,0)$,	$(4,-3,1,2)$,	$(4,-3,2,-1)$,
$(4,-3,2,1)$,	$(4,-2,-2,-2)$,	$(4,-2,-2,2)$,	$(4,-2,-1,-1)$,	$(4,-2,-1,1)$,	$(4,-2,0,0)$,
$(4,-2,1,-1)$,	$(4,-2,1,1)$,	$(4,-2,2,-2)$,	$(4,-2,2,2)$,	$(4,-1,-2,-1)$,	$(4,-1,-2,1)$,
$(4,-1,-1,-2)$,	$(4,-1,-1,0)$,	$(4,-1,-1,2)$,	$(4,-1,0,-1)$,	$(4,-1,0,1)$,	$(4,-1,1,-2)$,
$(4,-1,1,0)$,	$(4,-1,1,2)$,	$(4,-1,2,-1)$,	$(4,-1,2,1)$,	$(4,0,-2,0)$,	$(4,0,-1,-1)$,
$(4,0,-1,1)$,	$(4,0,0,-2)$,	$(4,0,1,-1)$,	$(4,1,-2,-1)$,	$(4,1,-2,1)$,	$(4,1,-1,-2)$,
$(4,1,-1,0)$,	$(4,1,-1,2)$,	$(4,1,0,-1)$,	$(4,1,1,-2)$,	$(4,1,2,-1)$,	$(4,2,-2,-2)$,
$(4,2,-2,2)$,	$(4,2,-1,-1)$,	$(4,2,-1,1)$,	$(4,2,1,-1)$,	$(4,2,2,-2)$,	$(4,3,-2,-1)$,
$(4,3,-2,1)$,	$(4,3,-1,-2)$,	$(4,3,-1,0)$,	$(4,3,-1,2)$,	$(4,3,0,-1)$,	$(4,3,1,-2)$,
$(4,3,2,-1)$,	$(4,4,-2,0)$,	$(4,4,-1,-1)$,	$(4,4,-1,1)$,	$(4,4,0,-2)$,	$(4,4,1,-1)$.

Finally, we look at the dynamic case for retrograde motion, then the selection rules are shown by:

- We cannot have positive integers for n and k and negative for m, because $\omega_\phi < 0$
- The general selection rule: $k + m + s = \text{even}$
- Take n to be positive because everything times - 1 gives the same resonance
- if $n = 0$, take k to be positive because everything times -1 gives the same resonance
- if $n = 0$ and $k = 0$, take m to be positive because everything times -1 gives the same resonance
- if $n = 0$, $k = 0$ and $m = 0$, take s to be positive because everything times -1 gives the same resonance
- multiple of one n, k, m, s combination do not contribute, we only consider the lowest order

The number of (n, k, m) combinations for the dynamic case in retrograde motion is also 354, and they are given by:

$(0,0,1,1)$,	$(0,1,-2,-1)$,	$(0,1,-1,-2)$,	$(0,1,0,-1)$,	$(0,1,1,-2)$,	$(0,1,1,0)$,
$(0,1,1,2)$,	$(0,1,2,-1)$,	$(0,1,2,1)$,	$(0,2,-2,-2)$,	$(0,2,-1,-1)$,	$(0,2,1,-1)$,
$(0,2,1,1)$,	$(0,2,2,-2)$,	$(0,2,2,2)$,	$(0,3,-2,-1)$,	$(0,3,-1,-2)$,	$(0,3,0,-1)$,
$(0,3,1,-2)$,	$(0,3,1,0)$,	$(0,3,1,2)$,	$(0,3,2,-1)$,	$(0,3,2,1)$,	$(0,4,-1,-1)$,
$(0,4,0,-2)$,	$(0,4,1,-1)$,	$(0,4,1,1)$,	$(0,4,2,0)$,	$(1,-4,-2,-2)$,	$(1,-4,-2,0)$,
$(1,-4,-2,2)$,	$(1,-4,-1,-1)$,	$(1,-4,-1,1)$,	$(1,-4,0,-2)$,	$(1,-4,0,0)$,	$(1,-4,0,2)$,
$(1,-4,1,-1)$,	$(1,-4,1,1)$,	$(1,-4,2,-2)$,	$(1,-4,2,0)$,	$(1,-4,2,2)$,	$(1,-3,-2,-1)$,
$(1,-3,-2,1)$,	$(1,-3,-1,-2)$,	$(1,-3,-1,0)$,	$(1,-3,-1,2)$,	$(1,-3,0,-1)$,	$(1,-3,0,1)$,
$(1,-3,1,-2)$,	$(1,-3,1,0)$,	$(1,-3,1,2)$,	$(1,-3,2,-1)$,	$(1,-3,2,1)$,	$(1,-2,-2,-2)$,
$(1,-2,-2,0)$,	$(1,-2,-2,2)$,	$(1,-2,-1,-1)$,	$(1,-2,-1,1)$,	$(1,-2,0,-2)$,	$(1,-2,0,0)$,
$(1,-2,0,2)$,	$(1,-2,1,-1)$,	$(1,-2,1,1)$,	$(1,-2,2,-2)$,	$(1,-2,2,0)$,	$(1,-2,2,2)$,
$(1,-1,-2,-1)$,	$(1,-1,-2,1)$,	$(1,-1,-1,-2)$,	$(1,-1,-1,0)$,	$(1,-1,-1,2)$,	$(1,-1,0,-1)$,
$(1,-1,0,1)$,	$(1,-1,1,-2)$,	$(1,-1,1,0)$,	$(1,-1,1,2)$,	$(1,-1,2,-1)$,	$(1,-1,2,1)$,
$(1,0,-2,-2)$,	$(1,0,-1,-1)$,	$(1,0,0,-2)$,	$(1,0,1,-1)$,	$(1,0,1,1)$,	$(1,0,2,-2)$,
$(1,0,2,0)$,	$(1,0,2,2)$,	$(1,1,-2,-1)$,	$(1,1,-1,-2)$,	$(1,1,0,-1)$,	$(1,1,1,-2)$,
$(1,1,1,0)$,	$(1,1,1,2)$,	$(1,1,2,-1)$,	$(1,1,2,1)$,	$(1,2,-2,-2)$,	$(1,2,-1,-1)$,
$(1,2,0,-2)$,	$(1,2,1,-1)$,	$(1,2,1,1)$,	$(1,2,2,-2)$,	$(1,2,2,0)$,	$(1,2,2,2)$,
$(1,3,-2,-1)$,	$(1,3,-1,-2)$,	$(1,3,0,-1)$,	$(1,3,1,-2)$,	$(1,3,1,0)$,	$(1,3,1,2)$,
$(1,3,2,-1)$,	$(1,3,2,1)$,	$(1,4,-2,-2)$,	$(1,4,-1,-1)$,	$(1,4,0,-2)$,	$(1,4,1,-1)$,
$(1,4,1,1)$,	$(1,4,2,-2)$,	$(1,4,2,0)$,	$(1,4,2,2)$,	$(2,-4,-2,0)$,	$(2,-4,-1,-1)$,
$(2,-4,-1,1)$,	$(2,-4,0,-2)$,	$(2,-4,0,2)$,	$(2,-4,1,-1)$,	$(2,-4,1,1)$,	$(2,-4,2,0)$,
$(2,-3,-2,-1)$,	$(2,-3,-2,1)$,	$(2,-3,-1,-2)$,	$(2,-3,-1,0)$,	$(2,-3,-1,2)$,	$(2,-3,0,-1)$,
$(2,-3,0,1)$,	$(2,-3,1,-2)$,	$(2,-3,1,0)$,	$(2,-3,1,2)$,	$(2,-3,2,-1)$,	$(2,-3,2,1)$,
$(2,-2,-2,-2)$,	$(2,-2,-2,2)$,	$(2,-2,-1,-1)$,	$(2,-2,-1,1)$,	$(2,-2,0,0)$,	$(2,-2,1,-1)$,
$(2,-2,1,1)$,	$(2,-2,2,-2)$,	$(2,-2,2,2)$,	$(2,-1,-2,-1)$,	$(2,-1,-2,1)$,	$(2,-1,-1,-2)$,
$(2,-1,-1,0)$,	$(2,-1,-1,2)$,	$(2,-1,0,-1)$,	$(2,-1,0,1)$,	$(2,-1,1,-2)$,	$(2,-1,1,0)$,
$(2,-1,1,2)$,	$(2,-1,2,-1)$,	$(2,-1,2,1)$,	$(2,0,-1,-1)$,	$(2,0,0,-2)$,	$(2,0,1,-1)$,
$(2,0,1,1)$,	$(2,0,2,0)$,	$(2,1,-2,-1)$,	$(2,1,-1,-2)$,	$(2,1,0,-1)$,	$(2,1,1,-2)$,

$(2,1,1,0)$,	$(2,1,1,2)$,	$(2,1,2,-1)$,	$(2,1,2,1)$,	$(2,2,-2,-2)$,	$(2,2,-1,-1)$,
$(2,2,1,-1)$,	$(2,2,1,1)$,	$(2,2,2,-2)$,	$(2,2,2,2)$,	$(2,3,-2,-1)$,	$(2,3,-1,-2)$,
$(2,3,0,-1)$,	$(2,3,1,-2)$,	$(2,3,1,0)$,	$(2,3,1,2)$,	$(2,3,2,-1)$,	$(2,3,2,1)$,
$(2,4,-1,-1)$,	$(2,4,0,-2)$,	$(2,4,1,-1)$,	$(2,4,1,1)$,	$(2,4,2,0)$,	$(3,-4,-2,-2)$,
$(3,-4,-2,0)$,	$(3,-4,-2,2)$,	$(3,-4,-1,-1)$,	$(3,-4,-1,1)$,	$(3,-4,0,-2)$,	$(3,-4,0,0)$,
$(3,-4,0,2)$,	$(3,-4,1,-1)$,	$(3,-4,1,1)$,	$(3,-4,2,-2)$,	$(3,-4,2,0)$,	$(3,-4,2,2)$,
$(3,-3,-2,-1)$,	$(3,-3,-2,1)$,	$(3,-3,-1,-2)$,	$(3,-3,-1,0)$,	$(3,-3,-1,2)$,	$(3,-3,0,-1)$,
$(3,-3,0,1)$,	$(3,-3,1,-2)$,	$(3,-3,1,0)$,	$(3,-3,1,2)$,	$(3,-3,2,-1)$,	$(3,-3,2,1)$,
$(3,-2,-2,-2)$,	$(3,-2,-2,0)$,	$(3,-2,-2,2)$,	$(3,-2,-1,-1)$,	$(3,-2,-1,1)$,	$(3,-2,0,-2)$,
$(3,-2,0,0)$,	$(3,-2,0,2)$,	$(3,-2,1,-1)$,	$(3,-2,1,1)$,	$(3,-2,2,-2)$,	$(3,-2,2,0)$,
$(3,-2,2,2)$,	$(3,-1,-2,-1)$,	$(3,-1,-2,1)$,	$(3,-1,-1,-2)$,	$(3,-1,-1,0)$,	$(3,-1,-1,2)$,
$(3,-1,0,-1)$,	$(3,-1,0,1)$,	$(3,-1,1,-2)$,	$(3,-1,1,0)$,	$(3,-1,1,2)$,	$(3,-1,2,-1)$,
$(3,-1,2,1)$,	$(3,0,-2,-2)$,	$(3,0,-1,-1)$,	$(3,0,0,-2)$,	$(3,0,1,-1)$,	$(3,0,1,1)$,
$(3,0,2,-2)$,	$(3,0,2,0)$,	$(3,0,2,2)$,	$(3,1,-2,-1)$,	$(3,1,-1,-2)$,	$(3,1,0,-1)$,
$(3,1,1,-2)$,	$(3,1,1,0)$,	$(3,1,1,2)$,	$(3,1,2,-1)$,	$(3,1,2,1)$,	$(3,2,-2,-2)$,
$(3,2,-1,-1)$,	$(3,2,0,-2)$,	$(3,2,1,-1)$,	$(3,2,1,1)$,	$(3,2,2,-2)$,	$(3,2,2,0)$,
$(3,2,2,2)$,	$(3,3,-2,-1)$,	$(3,3,-1,-2)$,	$(3,3,0,-1)$,	$(3,3,1,-2)$,	$(3,3,1,0)$,
$(3,3,1,2)$,	$(3,3,2,-1)$,	$(3,3,2,1)$,	$(3,4,-2,-2)$,	$(3,4,-1,-1)$,	$(3,4,0,-2)$,
$(3,4,1,-1)$,	$(3,4,1,1)$,	$(3,4,2,-2)$,	$(3,4,2,0)$,	$(3,4,2,2)$,	$(4,-4,-2,0)$,
$(4,-4,-1,-1)$,	$(4,-4,-1,1)$,	$(4,-4,0,-2)$,	$(4,-4,0,2)$,	$(4,-4,1,-1)$,	$(4,-4,1,1)$,
$(4,-4,2,0)$,	$(4,-3,-2,-1)$,	$(4,-3,-2,1)$,	$(4,-3,-1,-2)$,	$(4,-3,-1,0)$,	$(4,-3,-1,2)$,
$(4,-3,0,-1)$,	$(4,-3,0,1)$,	$(4,-3,1,-2)$,	$(4,-3,1,0)$,	$(4,-3,1,2)$,	$(4,-3,2,-1)$,
$(4,-3,2,1)$,	$(4,-2,-2,-2)$,	$(4,-2,-2,2)$,	$(4,-2,-1,-1)$,	$(4,-2,-1,1)$,	$(4,-2,0,0)$,
$(4,-2,1,-1)$,	$(4,-2,1,1)$,	$(4,-2,2,-2)$,	$(4,-2,2,2)$,	$(4,-1,-2,-1)$,	$(4,-1,-2,1)$,
$(4,-1,-1,-2)$,	$(4,-1,-1,0)$,	$(4,-1,-1,2)$,	$(4,-1,0,-1)$,	$(4,-1,0,1)$,	$(4,-1,1,-2)$,
$(4,-1,1,0)$,	$(4,-1,1,2)$,	$(4,-1,2,-1)$,	$(4,-1,2,1)$,	$(4,0,-1,-1)$,	$(4,0,0,-2)$,
$(4,0,1,-1)$,	$(4,0,1,1)$,	$(4,0,2,0)$,	$(4,1,-2,-1)$,	$(4,1,-1,-2)$,	$(4,1,0,-1)$,
$(4,1,1,-2)$,	$(4,1,1,0)$,	$(4,1,1,2)$,	$(4,1,2,-1)$,	$(4,1,2,1)$,	$(4,2,-2,-2)$,
$(4,2,-1,-1)$,	$(4,2,1,-1)$,	$(4,2,1,1)$,	$(4,2,2,-2)$,	$(4,2,2,2)$,	$(4,3,-2,-1)$,
$(4,3,-1,-2)$,	$(4,3,0,-1)$,	$(4,3,1,-2)$,	$(4,3,1,0)$,	$(4,3,1,2)$,	$(4,3,2,-1)$,
$(4,3,2,1)$,	$(4,4,-1,-1)$,	$(4,4,0,-2)$,	$(4,4,1,-1)$,	$(4,4,1,1)$,	$(4,4,2,0)$.

Finally, in listing 1 we show the Mathematica code used for selecting the relevant resonance number combinations, specifically for the dynamic case in retrograde motion. This case was chosen because it includes the most important features of the selection process and it is shown to demonstrate how the selection process is done in Mathematica.

```
(*Retrograde, so omegaphi is negative*)
rawnums=Flatten[Table[{n,k,m,s},{n,-4,4},{k,-4,4},{m,-2,2},{s,-2,2}],3];
filter1 = Select[rawnums,!(#[[1]]>=0&& #[[2]]>=0&& #[[3]]<=0 && #[[4]]>=0)&]; (* we can't have only positive numbers (but \[Omega]_phi is always negative for retrograde, so #3<=0) *)
filter2= Select[filter1,!(#[[1]]<=0&& #[[2]]<=0&& #[[3]]>=0&& #[[4]]<=0)&]; (* we can't have only negative numbers (but \[Omega]_phi is always negative for retrograde, so #3>=0)*)
filter3 = Select[filter2,EvenQ[#[[2]]+#[[3]]+#[[4]]]&];(* general selection rule: k+m+s=even *)
filter4 = Select[filter3,#[[1]]>=0&]; (*take n to be positive, because everything times -1 gives the same resonance*)
filter5  = Select[filter4,{#[[1]]==0,#[[2]]<0}!={True,True}&]; (*if n=0, take k to be positive because everything times -1 gives the same resonance*)
filter6 = Select[filter5,{#[[1]]==0,#[[2]]==0,#[[3]]<0}!={True,True,True}&]; (*if n=0 and k=0, take m to be positive because everything times -1 gives the same resonance*)
filter7 = Select[filter6,{#[[1]]==0,#[[2]]==0,#[[3]]==0,#[[4]]<0}!={True,True,True,True}&];(*if n=0 and k=0,m=0, take s to be positive because everything times -1 gives the same resonance*)
filter8=Select[filter7, MemberQ[filter7, {#[[1]]/2, #[[2]]/2, #[[3]]/2, #[[4]]/2}]!=True &];(*Check if element is multiple of another element*)
filter900=Select[filter8, MemberQ[filter8, {#[[1]]/3, #[[2]]/3, #[[3]]/3, #[[4]]/3}]!=True &] (*Check if element is multiple of another element*)
Print["The number of nkms combinations in general is ", Length[filter900]]
```

Listing 1: *Mathematica code: Selecting the relevant resonance number combinations in the dynamic case for retrograde motion*